Received: 7 December 2018 | Revised: 21 January 2019 | Accepted: 27 January 2019

DOI: 10.1002/aoc.4871

WILEY Applied Organometallic Chemistry

FULL PAPER

Spectroscopic investigation, DFT, fluorescence, molecular docking and biological studies of divalent and trivalent binuclear complexes prepared from benzoyl thiosemicarbazide derivative of 2-benzylmalonohydrazide

Reham M. El-Morshedy[1] | Mohammed M. El-Gamil[2] | Mohamed Mahmoud Abou-Elzahab[1] | Gaber M. Abu El-Reash[1]

[1]Department of Chemistry, Faculty of Science, Mansoura University, Mansoura, P.O.Box 70, Mansoura, Egypt

[2]Department of Toxic and Narcotic Drug, Forensic Medicine, Mansoura Laboratory, Medico legal Organization, Ministry of Justice, Egypt

Correspondence
Gaber M. Abu El-Reash, Department of Chemistry, Faculty of Science, Mansoura University, Mansoura, P.O.Box 70, Mansoura, Egypt.
Email: gaelreash@mans.edu.eg

The binuclear Cr (III), Mn (II) and Fe (III) complexes of *N,N′*-(2,2′-(2-benzylmalonyl)bis (hydrazine-1-carbonothioyl))dibenzamide (H_4BPCD), which derived from the combination of 2-benzylmalonohydrazide suspension with benzoyl-isothiocyanate, have been isolated and investigated by the necessary analytical and spectroscopic techniques. The IR studies show that H_4BPCD dispose as a mono-negative hexadentate ligand $(NOS)_2$ towards Mn (II) ion and tetra-negative hexadentate $(NOS)_2$ towards both Cr (III) and Fe (III) ions. The values of molar conductance in DMSO suggested the non-electrolytic nature for all complexes. The magnetic measurements and the electronic transitions data confirmed the hexa-coordinate geometry of complexes. The DFT geometry optimization of all compounds and IR comparative study of both theoretical and experimental of H_4BPCD were carried out. Moreover, the H_4BPCD and its Cr (III) complex displayed intra ligand ($\pi \rightarrow \pi^*$) fluorescence emission spectra which corroborate their photoactive nature. The coordinated and crystalline water molecules have been investigated by (TG/DTG) studies. The kinetic and thermodynamic parameters were computed using Horowitz- Metzger, Coats-Redfern and Broido methods. Biological studies of DNA binding, minimum inhibitory concentration, *in vitro* determination of SOD-like activity and MTT-cytotoxicity assay as well as molecular docking studies were tested for the ligand and its complexes.

KEYWORDS
DNA binding, molecular docking, MTT-cytotoxicity assay, spectral characterization, thiosemicarbazide

1 | INTRODUCTION

The N-, O- and S- containing ligands of dihydrazide derivatives that can chelate with two metal ions have become highly important because of symmetric and asymmetric binuclear complexes exhibited a variety of stereochemistries and bonding behaviors that produce diverse structures and properties.[1–3] Several studies have been carried out on the binuclear complexes because their interesting applications like creation of supramolecular structures to mimic metalloproteins,[4] DNA binding,[5] specific and selective catalysis,[6,7] sequestering of metal

ions and other of both biological and industrial applications. *In vitro* and *in vivo* tests[8] proved that dihydrazides possess non-genotoxic, anti-inflammatory, antioxidant and anticancer activities.[9–12] Also, their derivatives in the field of analytical chemistry used as reagents for specific chemical separations,[13–15] spectrophotometric microdetermination of some metal ions[16–18] and used for polymer industry.[19,20] Furthermore, luminescent compounds are very interesting because of their many applications for photocatalysis.[21–24]

Because the promotive application studies of malono hydrazide derivatives and their complexes[25] we have prepared *N,N′*-(2,2′-(2-benzylmalonyl)bis (hydrazine-1-carbonothioyl))dibenzamide (H_4BPCD) and its Cr (III), Mn (II) and Fe (III) complexes. The necessary studies of analytical, spectral, thermal, fluorescence and magnetic were carried out.

We apply geometry optimization (using Materials Studio package[26]) and conformational analysis to the H_4BPCD and all their possible structural isomers and have got the more stabilized. The proposed structures were upheld by DFT molecular modeling of the prepared compounds. Other studies carried out such as spectroscopic (IR,UV–vis, fluorescence, ^{1}H and ^{13}C NMR), magnetic calculations and thermal kinetics of the isolated complexes as well as its MIC efficacies as anti-bacterial and as anti-fungal microorganism were tested. Several transition metal complexes with flexible geometric transformation around the metal center especially Mn, Cu or Zn exhibit SOD activity[27,28] so, the determination of SOD-like activity and DNA-binding affinity are discussed. While, Molecular Docking was a powerful approach for structure-based drug discovery so, molecular docking studies carried out.

2 | EXPERIMENTAL

2.1 | Instrumentation and materials

The diethyl 2-benzylmalonate and hydrazine were purchased from Cambrian and Fluka and used as received. The analysis of C, H and N is carried out with a "Perkin–Elmer 2400 series II analyzer". The metal and chloride contents in prepared complexes were determined by traditional methods.[29] "*Fisher-Johns* melting point apparatus" is used for melting points (°C) determination and are uncorrected. The ^{1}H and ^{13}C NMR spectrum of H_4BPCD at room temperature was recorded on a Varian Gemini spectrometer (400 MHz) in d_6-DMSO at Faculty of Science, Kafr Elsheikh University using tetra methyl silane as an internal standard. IR spectra (4000–400 cm^{-1}) with KBr discs were recorded on a Mattson 5000 FTIR spectrophotometer. The electronic spectra of the complexes have been measured in the range 200–900 nm in DMSO solution on a Perkin Elmer Lamda 25 U*V*/Vis Spectrophotometer, at Mansoura University. The effective magnetic moment, μ_{eff}, per metal atom was measured by Gouy method on Sherwood scientific magnetic susceptibility balance at room temperature. The photoluminescent properties of all compounds were studied using a LS50B Jenway 6270 Fluorimeter. The TG and DTA in the temperature region (20-1000 °C) is carried out by Shimadzu thermogravimetric analyzer at a heating rate of 15 °C/min and nitrogen flow rate of 20 ml/min.

2.2 | Synthesis of *N,N′*-(2,2′-(2-benzylmalonyl)bis (hydrazine-1-carbonothioyl))dibenzamide (H_4BPCD)

The ligand was prepared in two main steps: Step1, of preparation the hydrazide by mixing 1: 2 molar ratio of diethyl 2-benzylmalonate (2.35 g, 0.01 mol) and hydrazine (0.486 g, 0.02 mol) with stirring for 2 minutes then adding 30 ml ethanol to the mixture followed by reflux for 2–3 hr, then the contents were poured in a beaker and left overnight. The solvent is removed by filtration and the residue washed by diethyl ether. Step 2, of preparation of H_4BPCD where ethanolic solution of benzoyl isothiocyanate (3.2778 g, 2.7 ml) is added to ethanolic suspension of hydrazide obtained (2.0891 g) and the mixture is refluxed for 3–4 hr. The obtained precipitate washed by diethyl ether and checked by TLC (Figure 1). The melting points of the hydrazide and H_4BPCD found to be 167 and 220 °C respectively.

2.3 | Synthesis of Cr (III), Mn (II) and Fe (III) complexes

The chloride salt of each concerning metal (1.02 mmol) dissolved in hot ethanol (30 ml) and then added to a hot ethanolic suspension of H_4BPCD (1.02 mmol,10 ml).

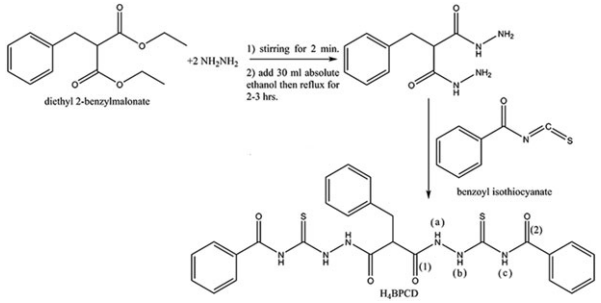

FIGURE 1 Preparation of H_4BPCD ligand

The contents were boiled for 4 hr. The fine formed precipitate was filtered and washed with ether and then desiccated over $CaCl_2$. Complexes powders in varying yields (80–91%) and the proposed structures are supported by analytical and spectroscopic data.

2.4 | Computational details

So as to get insight to the structural stabilities of the prepared compounds, DFT calculations with periodic boundary conditions were performed with the DMol^3[30] code, using Materials Studio package.[26] All the functions were used in conjunction with the precise double numerical plus polarization basis set DNP which is overweight the accuracy of than Gaussian basis sets.[31] The RPBE functional[32] is so far the best exchange-correlation functional,[33] in the light of the summed up gradient approximation (GGA), is utilized to assess the exchange and relationship effects of electrons. The geometric optimization is done with no symmetry limitation.

2.5 | Biological studies and molecular docking

2.5.1 | Biological studies

Minimum inhibitory concentration (MIC)

The potencies of H_4BPCD and it's complexes as antibacterial and antifungal were examined by diffusion method of agar and potato dextrose, respectively.[34] The examination was carried out in DMSO at 100, 200 and 500 μg/ml by using two bacteria (*Escherichia coli* as Gram-negative bacteria and *Staphylococcus aureus* as Gram-positive bacteria) and one fungi (*Candida albicans*) by the MIC method.[35] These bacterial strains were incubated for 24 h at 37 °C while fungi strain were hatched for 48 hr, at 37 °C. The Ampicillin and Clotrimazole as standerds were utilized for examination at the same conditions. Efficacy was estimated by diameter measuring of complete inhibition zone (mm).

Antioxidant activity (determination of SOD-like activity)

Free ligand (H_4BPCD) and it's complexes were investigated for Superoxide dismutase (SOD)-like activity using well-known method.[27] The solutions of H_4BPCD and/or its isolated complexes were prepared in DMSO. The response was started by phenazine methosulfate (PMS) addition, and the expansion in absorbance at 560 nm was recorded by the spectrophotometer for 5 minutes. For relative purposes, the activity of native $_L$-Ascorbic acid has also been resolved.

DNA-binding affinity

Colourimetric assay for DNA active compound were tested using the method reported by Burres N. *et al.*[36]

MTT-cytotoxicity assay[37]

HePG-2 cells were seeded in a 96-well plate at a density of $1.0x10^4$ cells/well[38] at 37 °C for 24 hr under 5% CO_2. The samples were dissolved in DMSO and diluted with phosphate buffer solution (PBS) to form concentration of 500, 200, 100, 50, 10 and 3 μmol/l. 5-fluorouracil was used as a standard anticancer drug for comparison. The different concentration of prepared samples were added to each well and were cultured for 48 hr. The treated cells were washed with (PBS) and 100 μl of MTT solution (5 mg/ml MTT stock in PBS diluted to 1 mg/ml with 10% RPMI-1640 medium) was added to each well and incubated for 4 h at 37 ° C. Finally, 100 μL of DMSO was added and optical densities at 540 nm were measured using a plate reader (EXL 800). The relative cell viability in percentage was calculated as:

$$\text{Relative cell viability}\% = \frac{A_{540} \text{ of treated samples}}{A_{540} \text{ of untreated sample}} \times 100$$

2.5.2 | Molecular docking

Protein preparation

The three-dimensional complex structure of *E. coli* (PDB ID: 1C14-chain A) was downloaded from the Protein Data Bank.[39] The protein structures were prepared using the protein preparation wizard program from the Schrödinger suite[40] in which water molecules (> 5A radius) and small molecules present were removed from the structure part, disulphide bonds were created and hydrogens were added to the PDB structures. Restrained impref minimization with default settings was performed on the structure with optimized potentials for liquid simulations (OPLS-2005) force field. The resulting structures were used for receptor grid generation for docking.

Ligand preparation

The ligand compound (H_4BPCD) intended to be used for docking were prepared using default protocol of the Ligprep program[41] in the Schrödinger's suite. Glide program[42] in the Schrödinger's suite was used for docking studies. All compounds and reference drug (ampicillin) were docked to the target protein using the glide dock XP protocol without using perform post-docking minimization. Glide E-Model was used as ranking criteria for the best-docked compound.[43]

3 | RESULTS AND DISCUSSION

The elemental composition of the isolated compounds in addition to their physical properties are scheduled in Table 1, which are in a decent concurrence with the proposed chemical formulae. Sadly, single crystals of the studied compounds cannot be isolated. The complexes were found to be non-hygroscopic and hardly soluble in most organic solvents except DMSO and DMF.

3.1 | IR spectra

The IR spectral data provide us by the valuable information regarding functional groups. The main characteristic frequencies of H_4BPCD (Figure 2) and its concerned metal complexes (Figure S1–S3, supplementary materials) are summarized in Table 2. Because the symmetrical nature of both sides in the ligand and complexes, one absorption band is observed for most of the functional groups except when the environment varies because of chelation.

The H_4BPCD (Figure 3) exhibits broad band of medium intensity at 3223 cm^{-1} assigned for υ (OH) and sharp intense band at 1687 cm^{-1} may be due to overlapping of $\upsilon(C{=}O)_1$ and $\upsilon(C{=}O)_2$ bands. Appearance of υ(C-O) band at 1252 cm^{-1} in addition of two mentioned bands pointed to the presence of H_4BPCD in the two forms (keto and enol, Figure 4) which confirmed also by ^1H and ^{13}C NMR spectral analysis. The vibrations of $(NH)_a$ and $(NH)_b$ lies at 3191 and 3061 cm^{-1} and the band at 1602 cm^{-1} referred to $\upsilon(C{=}N)_1$ remains around the same position in Cr (III) and Mn (II) complexes.[44,45]

The δ(C=S) band, observed at the 850 cm^{-1} not change in $[Cr_2(BPCD)Cl_2(H_2O)_4].H_2O$ complex (Figure 5), because its un-participation in coordination and undergoing blue shifted in $[Mn_2(H_3BPCD)Cl_3(H_2O)_3].3H_2O$ spectrum (Figure 6). In $[Fe_2(BPCD)Cl_2(H_2O)_4].5H_2O$ (Figure 7) complex, the dissaperance of the same band is accompanied by appearance of a broad vibration at 1630 cm^{-1} assigned to new $\upsilon(C{=}N)_3$ due to the thiolization and deprotonation of (SH) group. The broadness at 1630 cm^{-1} may be attributed to overlapping of $\upsilon(C{=}N)_3^*$ with $\upsilon(C{=}N)_1^*$.

The appearance of new bands at 1573 and 1562 cm^{-1} belongs to new $(C{=}N)_2^*$ in both Cr (III) and Fe (III) complexes respectively as a result of enolization and deprotonation of $(C{=}O)_2$ group. The behavior is different in Mn (II) complex where one of both $(C{=}O)_2$ groups coordinate as carbonyl and its vibration is shifted to higher wavenumber (1677 cm^{-1}) with reduction of intensity while the other $(C{=}O)_2$ enolized and coordinated with deprotonation thereby new absorption band appeared at 1582 cm^{-1} assigned to $\upsilon(C{=}N)_2^*$. The new low frequency non-ligand bands in the region 426–584 cm^{-1} and observed in the spectra of complexes can be attributed to υ(M-S), (M-O) and (M-Cl).[46,47]

3.2 | ^1H and ^{13}C NMR of H_4BPCD

The ^1H NMR spectrum of H_4BPCD (Figure 8) shows three singlet signals at δ = 10.17, 11.19 and 11.81 ppm relative to TMS that disappear upon deuteration (Figure S4, supplementary materials). These signals attributed to $(NH)_a$, $(NH)_b$ and (OH) protons respectively.[48,49] The signals of NH groups appeared in high downfield frequencies because of formation of two hydrogen bond between N(36)-H(81) and N(11)-H(48). Appearance of (OH) signal at high frequency is additional evidence that the ligand present in enol form. The multiplets at 7.15–7.95 ppm belong to the protons of phenyl ring.[50] Doublet and triplet signals at 3.15–3.20 and 3.92–3.98 ppm refereed to $(\text{-}CH_2)$ and (-CH) groups respectively.

The ^{13}C NMR spectrum of H_4BPCD (Figure 9) shows two signals belong to $(C{=}O)_1$ and $(C{=}O)_2$ groups appear at δ = 172.01 and 164.55 ppm, and also a signal at δ = 175.45 ppm assigned to (C=S) group. The aromatic

TABLE 1 Analytical and physical data of H_4BPCD and its metal complexes

Compound Empirical Formula (F.Wt.)	Colour	M.P. (°C)	Yield (%)	Found (Calcd.) %				
				C	H	N	M	Cl
H_4BPCD $C_{26}H_{24}N_6O_4S_2$ (548.64)	white	220	95	56.81 (62.99)	4.45 (4.22)	15.54 (15.32)	- -	- -
$[Fe_2(BPCD)Cl_2(H_2O)_4].5H_2O$ $C_{26}H_{38}Cl_2Fe_2N_6O_{13}S_2$ (889.33)	Black	210	80	35.13 (35.11)	4.29 (4.31)	9.07 (9.08)	12.59 (12.56)	7.95 (7.97)
$[Mn_2(H_3BPCD)Cl_3(H_2O)_3].3H_2O$ $C_{24}H_{35}Cl_3Mn_2N_6O_{10}S_2$ (871.94)	Paige	230	91	35.75 (35.81)	4.15 (4.05)	9.58 (9.64)	12.15 (12.20)	12.25 (12.60)
$[Cr_2(BPCD)Cl_2(H_2O)_4].H_2O$ $C_{26}H_{30}Cl_2Cr_2N_6O_9S_2$ (807.97)	Olive	250	86	38.40 (38.57)	3.66 (3.74)	10.58 (10.38)	12.25 (12.85)	8.85 (8.76)

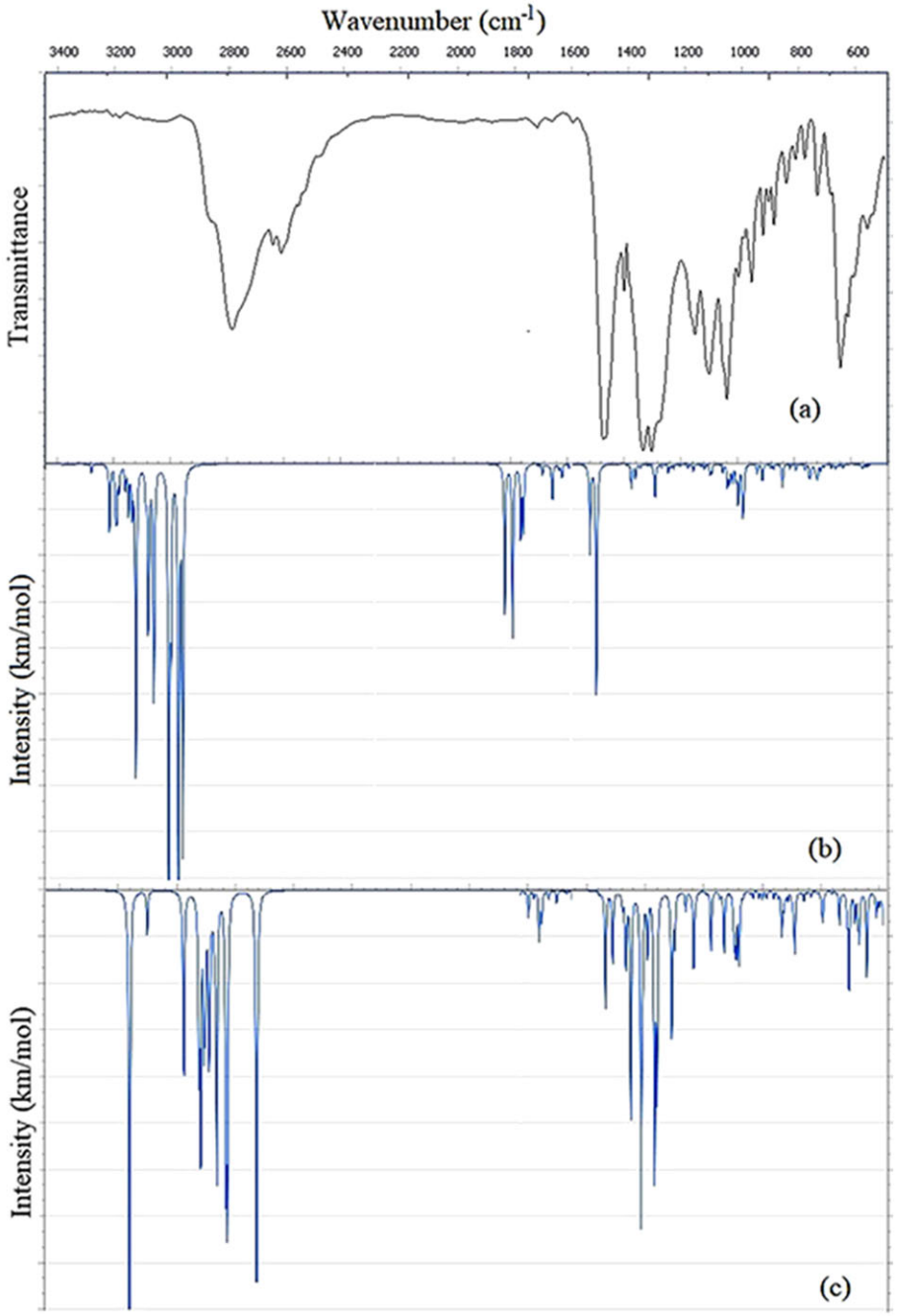

FIGURE 2 IR spectrum for H_4BPCD a) Experimental, b) Theoretical IR for H_4BPCD_{keto}, c) Theoretical IR for H_4BPCD_{enol}

carbons were observed at δ = 126.92–138.66.[51] Moreover appearance of carbon resonance signal of (N=C-OH) at 168.68 in addition of $(C=O)_1$ signal suggest the presence of keto-enol tautomers of in solution. Since the more available enol form leads to a decrease in polarization causing the downshift in the resonance of $(C=O)_1$ from 172.01 to 168.68. This suggestion is confirmed by energy gap (E_{HOMO} -E_{LUMO}) calculations where of enol form (0.897 ev) less than that for keto form (1.157 ev) which mean that it is more reactive, and hence that explains why chelation with metal ions takes place in enol form in all prepared complexes.

3.3 | Electronic spectra and magnetic behavior

The spectral data of H_4BPCD and its complexes are illustrated in Table 3. The ligand H_4BPCD shows two intense bands around 307 nm (32573 cm^{-1}) and 342 nm (29240 cm^{-1}) in DMSO solution, because of the intramolecular transitions (π–π*) and (n–π*) respectively. These transitions shifted to slightly higher wavenumbers in the complexes.[52,53]

The spectrum of the iron compound displays multiple bands belong to O_h environment at 17483, 23585, 24994

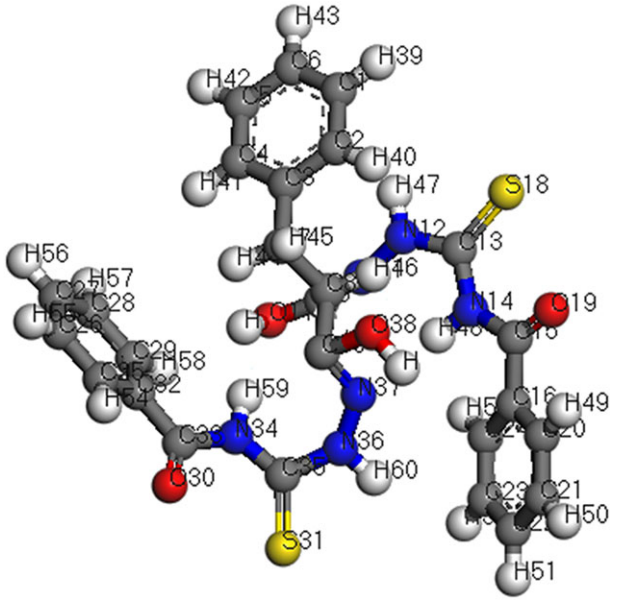

FIGURE 3 Molecular modeling of H_4BPCD_{enol} form (1)

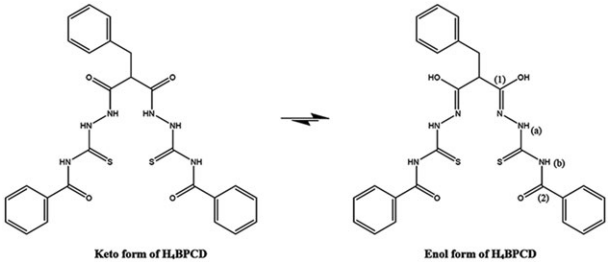

FIGURE 4 Keto/enol form of the title compound H_4BPCD

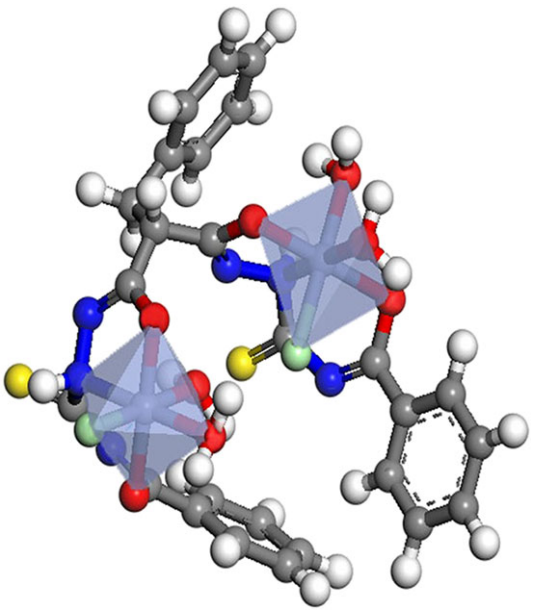

FIGURE 5 Molecular modeling of $[Cr_2(BPCD)Cl_2(H_2O)_4].H_2O$

and 27933 cm^{-1} which are attributed to $^6A_{1g} \rightarrow {}^4T_{1g}(G)$, $^6A_{1g} \rightarrow {}^4T_{2g}(G)$, $^6A_{1g} \rightarrow {}^4E_g(G)$ and $^6A_{1g} \rightarrow {}^4T_{2g}(D)$ transitions, respectively.[54] The measured μ_{eff} is found to be 5.6 B.M. which suggested the sp^3d^2 hybridization in Fe (III) ion.[55]

The diffused reflectance spectrum of the Mn (II) complex shows three bands at 17036, 19960 and 22696 cm^{-1} assignable to $^6A_{1g} \rightarrow {}^4T_{1g}$, $^6A_{1g} \rightarrow {}^4T_{2g}(G)$ and $^6A_{1g} \rightarrow {}^4E_g(G)$ transitions, respectively.[56] The magnetic moment value 4.8 B.M. indicates the occurrence of Mn (II) complex in O_h geometry.[54] However, the lowering of magnetic moment value than normal value may be due to the sharing of high diamagnetic sulphur atom of CS group in coordination. As noticed, there is no sextet spin multiplicity in any excited state, where the transitions from the ground state ($^6A_{1g}$) are expected to be spin-forbidden and both the band intensities and Molar absorptivity values (ε) are low.

The electronic spectrum of Cr (III) complex (μ_{eff} = 2.6 B.M.) demonstrates two bands at 25510 cm^{-1} (υ_2) and 28902 cm^{-1} (υ_3) allude to $^4A_{2g}(F) \rightarrow {}^4T_{1g}(F)$ and $^4A_{2g}(F) \rightarrow {}^4T_{1g}(p)$ transitions, separately, affirmed the octahedral geometry.[57] We could not observe υ_1 band which expected to be at ca. 451 nm (22163 cm^{-1}) for the $^4A_{2g}(F) \rightarrow {}^4T_{2g}(F)$ transition. The estimated values of Dq, β and B also coincident with O_h geometry.[58]

3.4 | Fluorescence studies

The emission spectra of H_4BPCD and its Cr (III) complex were measured upon the excitation wavelength around

TABLE 2 Assignment of the IR spectral bands of H_4BPCD and its metal complexes

Compound	υ(O-H)	$\upsilon(C=N)_1$	υ(C-O)	δ(C=S)	$\upsilon(C=O)_2$	$\upsilon(C=N)_2^*$	υ(C=C)	υ(N-N)	$\upsilon\ (NH)_a$	$\upsilon\ (NH)_b$
H_4BPCD (experimental)	3223	1602	1252	850	1687	-	1527	980	3191	3061
$[Fe_2(BPCD)Cl_2(H_2O)_4].5H_2O$	obs.	1630	1231	-	-	1562	1494	942	Obs.	-
$[Mn_2(H_3BPCD)Cl_3(H_2O)_3].3H_2O$	obs.	1604	1257	876	1677	1580	1495	950	3193	3062
$[Cr_2(BPCD)Cl_2(H_2O)_4].H_2O$	-	1605	1255	851	-	1573	1495	961	Obs.	-

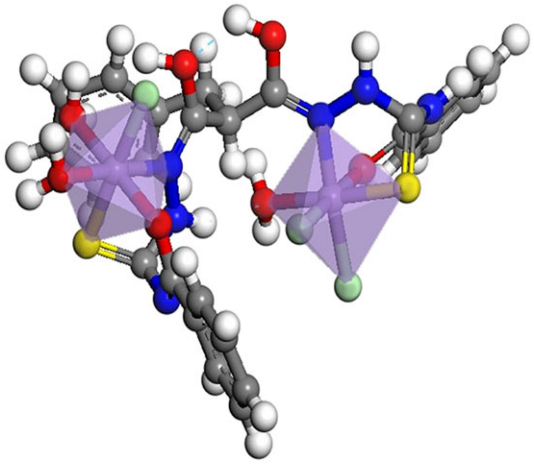

FIGURE 6 Molecular modeling of $[Mn_2(H_3BPCD)Cl_3(H_2O)_3].3H_2O$

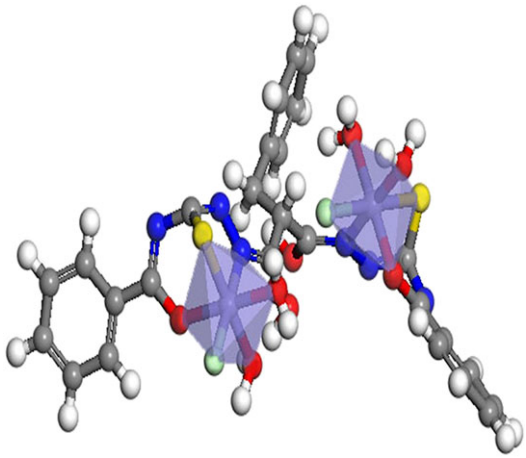

FIGURE 7 Molecular modeling of $[Fe_2(BPCD)Cl_2(H_2O)_4].5H_2O$

their maximum absorption. The spectra were recorded in DMSO at room temperature and depicted in Figure 10. Because the fluorescence intensities of the Mn (II) and Fe (III) complexes are much too weak therefore they cannot be discussed in our present work. The fluorescence spectrum of ligand displayed an emission band at 432 nm when excited at 309 nm that was attributed to the intra-ligand $\pi \rightarrow \pi^*$ transitions, while that for Cr (III) complex shows one emission band at 503 nm followed the excitation at 347 nm. It is noteworthy that the emission wavelength of Cr (III) complex is slightly longer than that of the free ligand, which is may be due to the chelation of the ligand to the metal center. Such chelation enhances the rigidity of the ligand and thus reduces the loss of energy by radiation less decay of the intra-ligand emission excited state. Thus, the ligand and its chromium complex may be used in further photochemical applications which are with great interest lately.

3.5 | Molecular modeling

3.5.1 | IR

Frequency calculation analyses have been performed for H_4BPCD possible forms in order to ensure the most prevalent form/forms. Because of large size of the molecule, calculated modes of vibrations are complex especially, the in plane, out of plane and torsion modes. The last kind is the most difficult to assign due to interference with the ring modes. However, there are some intense frequencies, useful for characterization in the IR spectrum. The little difference between that experimental wavenumbers and the calculated one is may due to that the experimental wavenumbers were carried out for solid samples, while the calculations were processed in a vacuum for a free molecule as shown in Figures 1b and 1c and Table 4. It was found that the values of wavenumbers of calculated frequencies are with good agreement with experimental one, especially combination with the two graphs of form 1 (enol form) and form 3 (keto form) which confirm the presence of the two forms in the solid form of the title compound.

The corresponding graphic described harmony between the experimental and theoretical wavenumbers (Figure 11) since the relations between them are linear and can be expressed by the next equations:

$$\text{For the enol form } \upsilon_{cal} = 0.99425\ \upsilon_{exp} + 11.352 \text{ with correlation coefficients } \times \left(R^2 = 0.99977\right).$$

$$\text{For the keto form } \upsilon_{cal} = 1.01121\ \upsilon_{exp} + 23.899 \text{ with correlation coefficients } \times \left(R^2 = 0.99918\right).$$

3.5.2 | Geometry optimization with DFT method

For ligand and its possible forms

The DFT/DMoL^3 method has been used for a complete study of the molecular structures of all the possible conformations of H_4BPCD (Figure 12) in order to obtain their stability order according to the calculated energy components in addition of spin polarization as listed in Table 5. It was found that H_4BPCD form (1) has the lowest total energy and highest binding energy which mean that form (1) is the most stable conformation and that clarifies why all coordination modes takes place in this form.

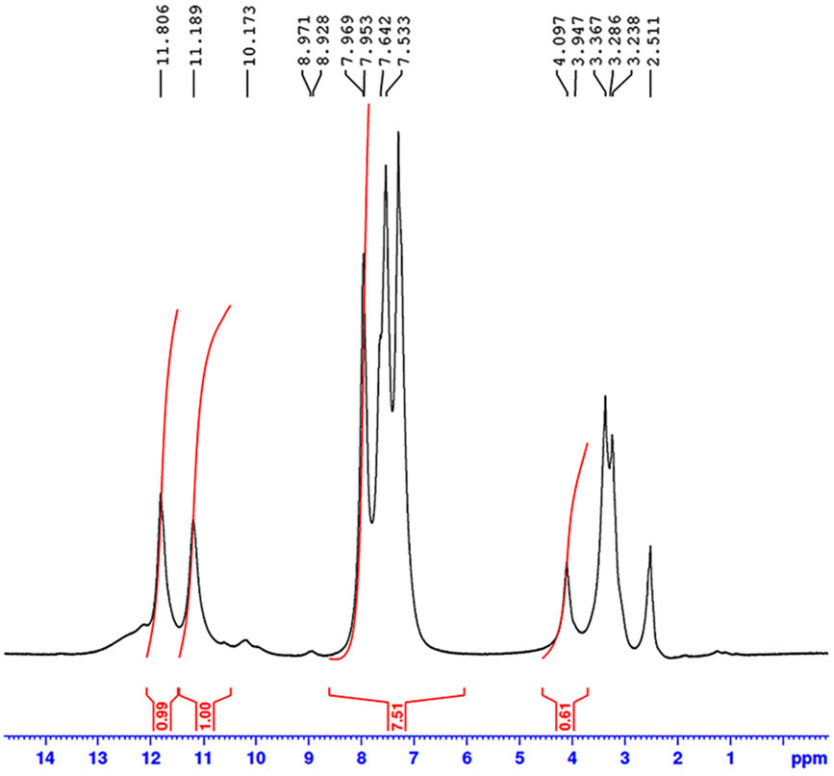

FIGURE 8 ^{1}H NMR spectrum of H_4BPCD

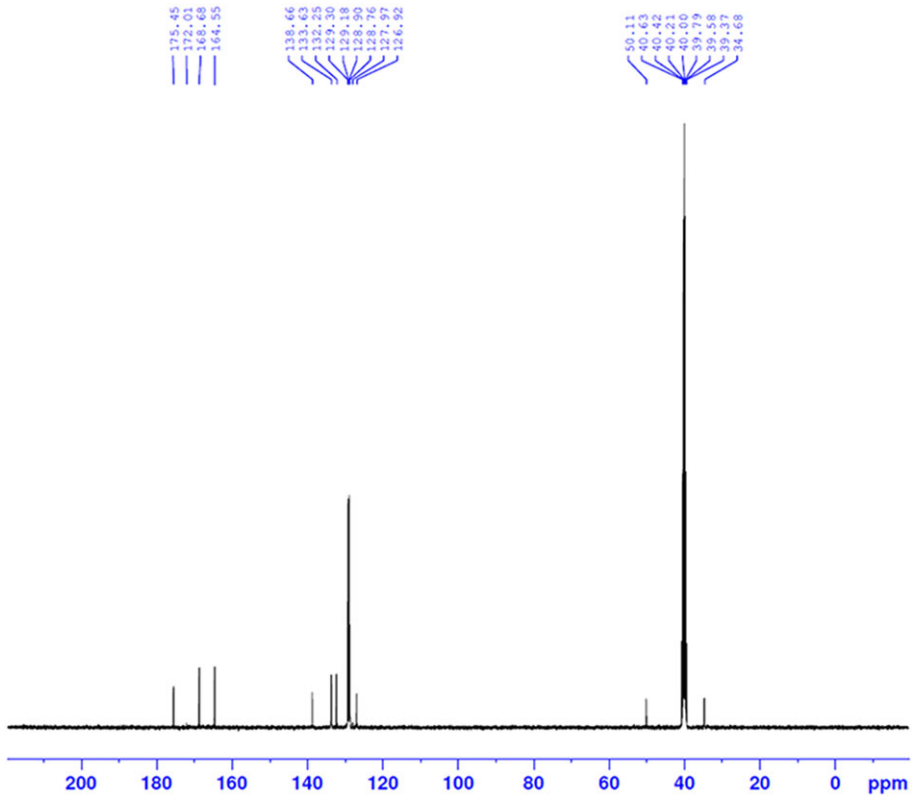

FIGURE 9 ^{13}C NMR spectrum of H_4BPCD

For ligand in enol form and its metal complexes

For the discussion of optimized molecular geometry of H_4BPCD and its metal complexes, bond lengths and angles are calculated and the data listed in Table S1, supplementary materials. There are some important remarks:

TABLE 3 Spectral absorption bands, magnetic moments and ligand field parameters of H_4BPCD and its metal complexes

Complex	λ_{max} nm	λ_{max} cm^{-1}	band assignment	Dq	B	β (B/B_o)	ε	μ_{eff} (B.M)	geometry
H_4BPCD	$342_{(m)}$	$29240_{(found)}$	(n–π*)	-	-	-	-	-	-
	$307_{(s)}$	$32573_{(found)}$		-	-	-	-	-	-
	$239_{(sh)}$	$41841_{(found)}$	(π–π*)	-	-	-	-	-	-
$[Cr_2(BPCD)Cl_2(H_2O)_4].H_2O$	451	$22163_{(calc.)}$	$^4A_{2g}(F) \rightarrow {}^4T_{2g}(F)(\upsilon_1)$ (υ_1)	2216	905	0.98	-	2.6	O_h
	$392_{(m)}$	$25510_{(found.)}$	$^4A_{2g}(F) \rightarrow {}^4T_{1g}(F)$ (υ_2)				1131		
	$346_{(s)}$	$28902_{(found)}$	$^4A_{2g}(F) \rightarrow {}^4T_{1g}(p)$ (υ_3)				2767.3		
$[Fe_2(H_2BPCD)Cl_4(H_2O)_2].5H_2O$	$572_{(w)}$	$17483_{(found)}$	$^6A_{1g} \rightarrow {}^4T_{1g}(G)$ (υ_1)	801.3	728.5	0.76	463.6	5.6	O_h
	$424_{(s)}$	$23585_{(found)}$	$^6A_{1g} \rightarrow {}^4T_{2g}(G)$ (υ_2)				2096		
	$400_{(s)}$	$24994_{(found)}$	$^6A_{1g} \rightarrow {}^4E_g(G)$ (υ_3)				1910		
	$358_{(s)}$	$27933_{(found)}$	$^6A_{1g} \rightarrow {}^4T_{2g}(D)$ (υ_4)				2949		
$[Mn_2(H_3BPCD)Cl_3(H_2O)_3].3H_2O$	$587_{(w)}$	$17036_{(found)}$	$^6A_{1g} \rightarrow {}^4T_{1g}(G)$ (υ_1)	780.8	709.8	0.74	30.4	4.8	O_h
	$501_{(m)}$	$19960_{(found)}$	$^6A_{1g} \rightarrow {}^4T_{2g}(G)$ (υ_2)				30.42		
	$441_{(s)}$	$22696_{(found)}$	$^6A_{1g} \rightarrow {}^4E_g(G)$ (υ_3)				50.7		

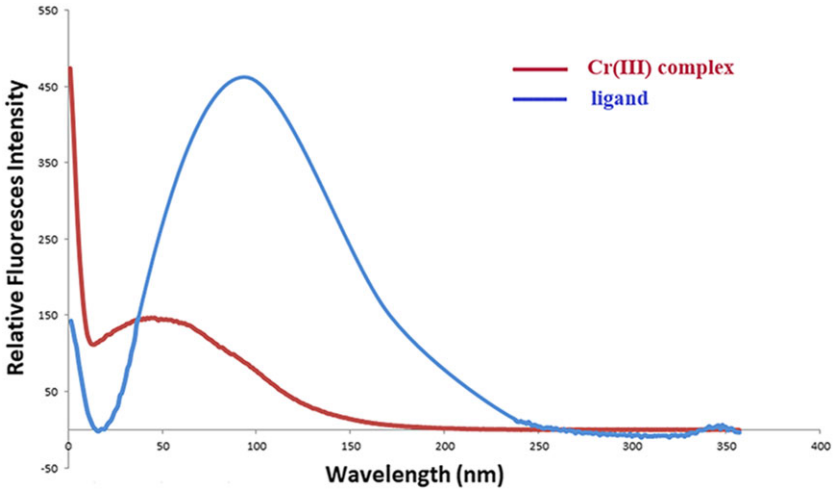

FIGURE 10 The fluorescence spectra of ligand and its Cr (III) complex

TABLE 4 Theoretical IR comparison of H_4BPCD possible forms

Compound	υ(O-H)	$\upsilon(C=N)_1$	υ(C-O)	δ(C=S)	υ(C-S)	υ(S-H)	$\upsilon(C=O)_1$	$\upsilon(C=O)_2$	$\upsilon(C-O)_2$	$\upsilon(C=N)_2$*	υ(C=C)	υ(N-N)	υ (NH)a	υ (NH)b
H_4BPCD (experimental)	3223	1602	1252	850	-	-	-	1687	-	-	1527	980	3196	3061
H_4BPCD_{enol} form1 (theoretical)	3195	1605	1266	851	-	-	-	1657	-	-	1527	981	3195	3061
H_4BPCD form2 (theoretical)	3300	1618	1252	843	-	-	-	-	1335	1585	1521	977	3177	3062
H_4BPCD_{keto} form3 (theoretical)	-	-	-	849	-	-	1740	1680	-	-	1524	981	3182	3065
H_4BPCD form4 (theoretical)	3259	1629	1268	855	1110	1229	-	1630	1366	-	1516	986	3167	3098
H_4BPCD form5 (theoretical)	-	-	-	-	1116	1259	1783	1668	-	-	1515	958	3193	3086

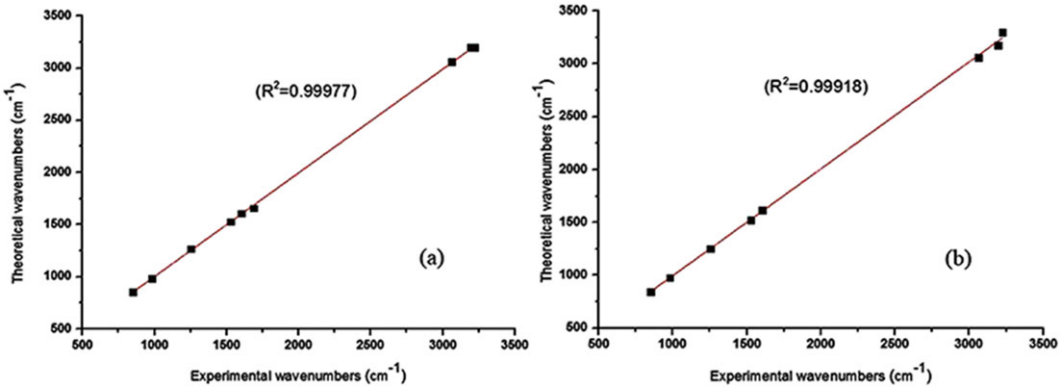

FIGURE 11 The linear regression between the experimental and theoretical frequencies of H_4BPCD a) for keto form and b) for enol form

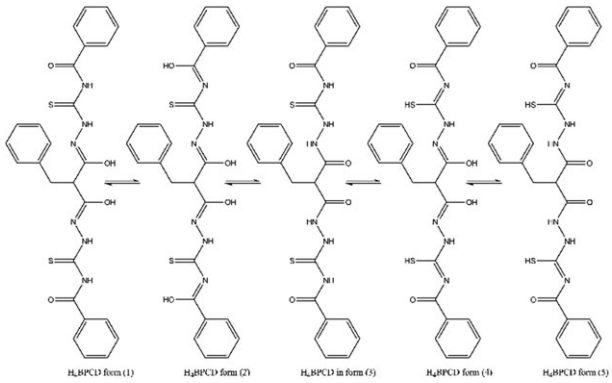

FIGURE 12 structure of possible conformations of H_4BPCD

1. The optimized $[C(10)\text{-}N(37)]_{azomethan)1)}$ and $[C(9)\text{-}N(11)]_{azomethan(1)}$ bond distances in the parent ligand elongated due to its coordination in the isolated complexes.
2. $(C\text{-}O)_1$ bond elongated only in $[Cr_2(BPCD)Cl_2(H_2O)_4].H_2O$ due to coordination *via* O(38) and O(17) of deprotonated OH groups.[59]
3. For (N-N) bond, become slightly longer in both $[Mn_2(H_3BPCD)Cl_3(H_2O)_3].3H_2O$ and $[Cr_2(BPCD)Cl_2(H_2O)_4].H_2O$ because of coordination *via* N(11), N(37) and N(12), N(36) respectively. On contrast, the bond become shorter in $[Fe_2(BPCD)Cl_2(H_2O)_4].5H_2O$. Moreover, (C=S) bond elongated also in Mn (II) complex because of coordination takes place from S(31).
4. C(15)-O(19) and C(33)-O(30) ketone-type in $[Cr_2(BPCD)Cl_2(H_2O)_4].H_2O$ and $[Fe_2(BPCD)Cl_2(H_2O)_4].5H_2O$, enolized resulting the disappearance of the double bond character over C(15)-O(19) and C(33)-O(30), and its appearance over N(14)-C(15) and N(34)-C(33). Also, absence of double bond character over both S(31)-C(35) and C(13)-S(18) and its appearance over N(12)-C(13) and C(35)-N(36) in Fe (III) complex.
5. Elongation and weakness of the (C-O) bond distances (in all complexes) as a result of formation of the M-O bond.[60]
6. As the result of coordination, the angles of ligand bonds are altered and the great change belong to N(34)-C(33)-O(30) and S(18)-C(13)-N(12) angles which are increased or reduced because the coordination.[60]
7. In all complexes the angle of bonds found to be in coincide with O_h geometry range expecting d^2SP^3 or SP^3d^2 hybridization.
8. The M-N, M-O and M-S bonds according to their lengths can be arranged as follows: S(31)-Fe(39) > S(18)-Fe(40) > Cr(40)-O(19) > O(38)-Cr(39) > O(17)-Cr(40) > O(19)-Mn(47) > O(30)-Mn(39) > O(19)-Fe(40) = O(30)-Fe(39) reflecting the great strength of the Fe-O and Mn-O bonds than the others. Finally for M-X bond, it obeys the order Cr-Cl > Fe-Cl > Mn-Cl. Due to the elongation in the bonds, vibration frequency need smaller energy and consequently appear at smaller frequency which is confirmed from the practically IR values.

3.5.3 | Chemical reactivity

Global reactivity descriptors

The highest occupied molecular orbital and the lowest-lying unoccupied molecular orbital (HOMO and LUMO respectively) are also named as frontier molecular orbitals (FMOs). The FMOs provide useful information about the reactivity and kinetic stability of compounds.[61–63] Surfaces for the frontier orbital were drawn for more understanding of the bonding scheme of the investigated compounds and it is shown in Figures 13 and 14 for ligand keto/enol forms and the other compounds in supplementary file (Figures S5-S7).

TABLE 5 Some energetic properties of H_4BPCD and its metal complexes calculated by $DMOL^3$ using DFT method

Compound	Energy components (kcal/mol)					Total Energy	Binding Energy (kcal/mol)	Dipole moment (D)			
	Sum of atomic energies	Kinetic Energy	Electrostatic energy	Exchange-correlation energy	Spin polarization energy			μ_x	μ_y	μ_z	μ_{Total}
H_4BPCD form (1)	−1518200.4	−11886.8	−17.3	2807.0	2233.2	−15258777	−6863.9	17.3	26.8	−3.0	18.9
H_4BPCD form (2)	−1518833.5	−11662.2	−548.4	2877.1	2287.9	−1525064.3	−7044.2	−0.8	0.8	5.0	5.03
H_4BPCD form (3)	−1517567.4	−12209.4	582.1	2744.8	2178.4	−1524262.6	−6695.2	12.3	−1.8	3.1	12.8
H_4BPCD form (4)	−1517567.4	−11863.3	260.2	2730.9	2178.4	−1524246.9	−6679.6	−8.3	−7.3	2.5	11.3
H_4BPCD form (4)	−1517567.4	−12211.8	614.9	2723.2	2178.4	−1524256.9	−6689.6	−6.1	3.4	−4.7	8.35
$[Cr_2(BPCD)Cl_2(H_2O)_4].H_2O$	−241560.5	−11624.3	−2539.4	3376.7	2723.9	−2423577.9	−8062.2	−23.5	7.2	12.5	27.5
$[Mn_2(H_3BPCD)Cl_3(H_2O)_3].3H_2O$	−2680811.6	−9775.7	−4549.7	3466.9	2774.8	−2688894.1	−8083.6	−4.6	17.9	−14.9	23.7
$[Fe_2(BPCD)Cl_2(H_2O)_4].5H_2O$	−2561210.5	−6445.6	−9020.8	3377.9	2861.1	−2570437.8	−9227.3	−0.2	−4.5	−7.0	8.28

The HOMO represents the electron donor orbital (π donor), while the LUMO represents the electron acceptor orbital (π acceptor). The negative sign of HUMO and LUMO energies and their neighboring orbitals indicate the stability of prepared molecules.[64]

According to calculation results, it was found that there is a rise in the value of E_{HOMO} adhere by lengthen (weakness) of the metal–ligand bonds leading to a shortness (strengthen) of the sites neighboring to the metal ligand centers.[65] The HOMO level is mostly localized on N(12),N(37), S(18), S(31),O(11), O(31), O(19) and O(30) showing they are the favored sites for nucleophilic attack at the central metal ion.

Moreover, the FMOs theory can anticipate coordination sites (or electrophilic attack) on aromatic compounds. An initial presumption is that – in many reactions – the reaction won't takes place until there is a maximum overlap reached between HOMO on one molecule, and the LUMO on the other. We can deduce that, by determining the largest value of molecular orbital coefficients from calculation which may be considered as the sites of coordination. It was found that the nitrogen of the ($C=N^1$) group, the sulphur of (C=S) group and the oxygen of ($C=O^2$) group largest value of molecular orbital coefficients. And this explains why metal atoms coordinate mostly to the ligand from these sites.

In addition to determining how the interaction occurs of the molecule with other species, the FMOs could also predict the chemical reactivity and kinetic stability of the molecule, optical polarizability and chemical hardness–softness of a molecule through their energy gap between HOMO and LUMO.[66,67]

Considering the chemical hardness, large ΔE means a hard compound, and small ΔE means a soft compound. Soft molecule favors easy polarization for both molecules, so they are more reactive than hard molecules since they could easily offer electrons to an acceptor.[68] This explains why H_4BPCD form (1) is the most reactive form and why chelates in this form in all complexes.

In the meantime the decrease of energy gap means that the final charge transfer takes place within the compound, which influences its biological activity. This conclusion proved by the comparison of biological study data with ΔE gap, the order of the compounds according to their ΔE gap calculations found to be as follow H_4BPCD > $[Fe_2(BPCD)Cl_2(H_2O)_4].5H_2O$ > $[Cr_2(BPCD)Cl_2(H_2O)_4].H_2O$ > $[Mn_2(H_3BPCD)Cl_3(H_2O)_3].3H_2O$ which is the same order of biological reactivity in all tested bio-activities. That means that we can predict the most reactive biological compounds with ΔE gap calculations before carrying out real tests.

According to the MOT, the electron affinity and ionization energy can be indicated by HOMO and LUMO

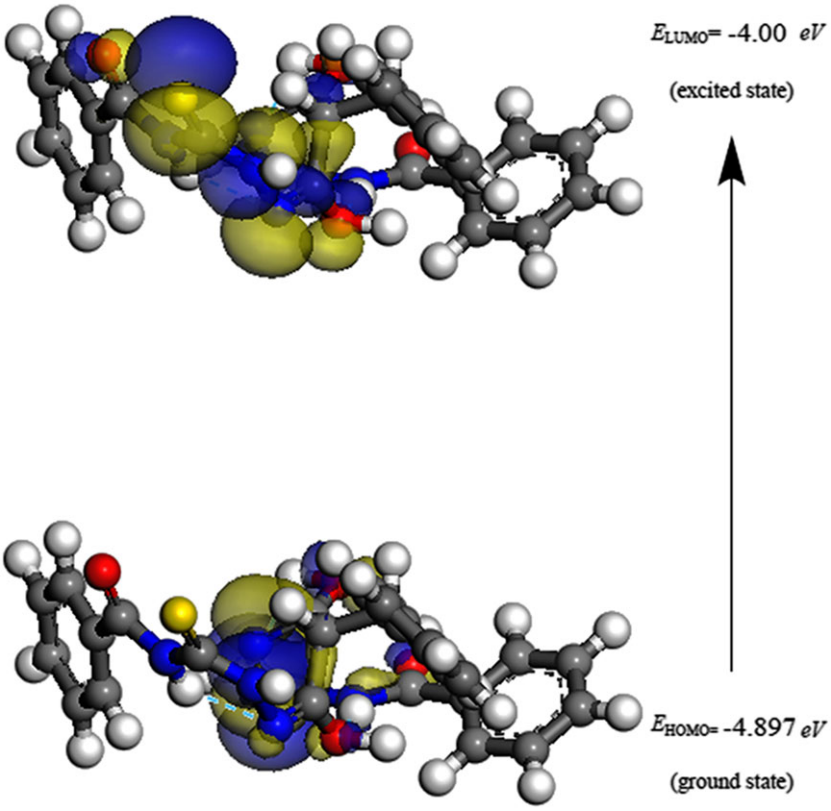

FIGURE 13 3D plots frontier orbital energies using DFT method for H_4BPCD (enol form)

energies as A = -E_{LUMO} and I = -E_{HUMO}, respectively. The electronegativity, $\chi = -1/2\ (E_{\mathrm{LUMO}} + E_{\mathrm{HOMO}})$, global hardness, $\eta = 1/2\ (E_{\mathrm{LUMO}} - E_{\mathrm{HOMO}})$. χ and η can also expressed in terms of A and I as:

$$\chi = \frac{(I+A)}{2} \text{ and } \eta = \frac{(I-A)}{2}$$

The chemical potential, $\mu = -\chi = 1/2\ (E_{\mathrm{LUMO}} + E_{\mathrm{HOMO}})$, global softness, $S = 1/2\ \eta$, the softness, $\sigma = 1/\eta$ and global electrophilicity index, $\omega = \mu^2/2\ \eta$.[69,70] These parameters have been evaluated and tabulated Table 6.

The atomic parameter linked with the energetics of removal of an electron is the ionization potential (I),[71] whereas that for the addition of an electron is electron affinity (A). Therefore, these two parameters deciding, somehow, the charge distribution and/or redistribution in molecular systems during molecular formation and hence chemical bonding as well as reactivity. The transfer of partial charge takes place in many bonds such as covalent and hydrogen bonds.[72]

The usefulness of electronegativity (χ) and absolute hardness (η) includes their ability to predict chemical activity.[73] For a given molecule it can be determined as Lewis acid or Lewis base according to its χ value. For bases, the χ values are small and large values characterize acids.[74] In between the molecules the transfer of electrons occurs from molecule with low χ to that with high χ. This fact agree well with results that parent molecule H_4BPCD have lowest value of χ so it could be considered as Lewis base (soft base). Thus Lewis base ligands are most efficacy for complex formation.[75] Thereby, it is deduced that the ligand with a proper softness (σ) value has a good propensity to coordinate metal ions effectively .[76] Moreover, according to electrophilicity index (ω) definition,[77] the ω measures the tendency of compound to gain electrons.

Local reactivity descriptors

Fukui function f (r) one of the most useful parameter in the identification of privileged sites of reactivity (active sites) in a molecule.[78–80] It is defined as:

$$f\ (\mathrm{r}, N) = \left(\frac{\partial(\partial E/\delta \upsilon_{ext})_N}{\partial N}\right)_{\upsilon_{ext}}$$

Where E is the energy, N the number of electrons, and υ_{ext} is the external potential. The local (condensed) Fukui functions (f_k^+, f_k^-, f_k^o) are calculated using conventional method.[70]

The results for H_4BPCD in enol form predict the highest f_k^+ value for N(37) indicates that it is the most probable site for nucleophilic attack. From the values

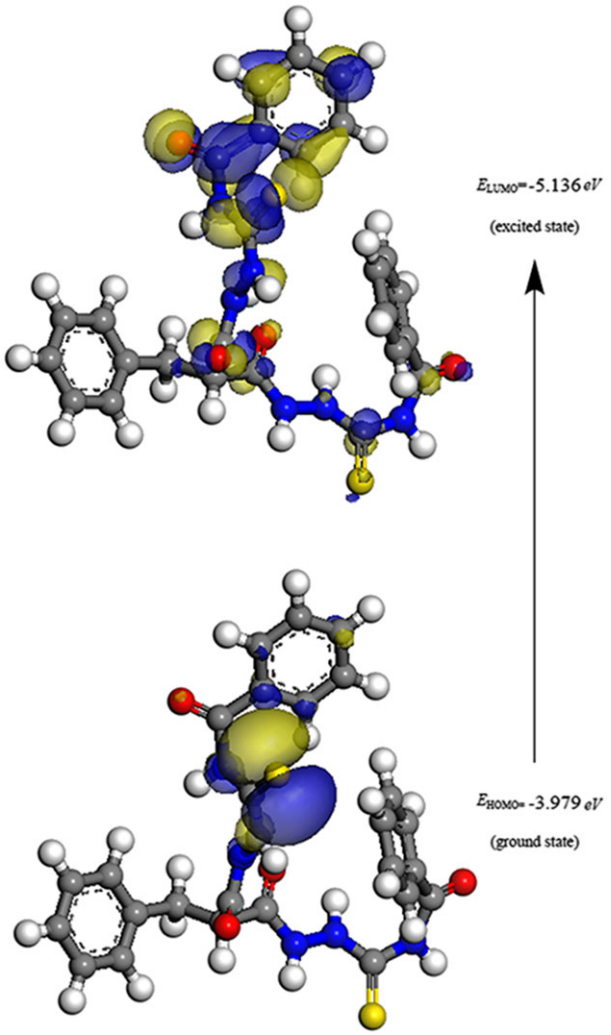

FIGURE 14 3D plots frontier orbital energies using DFT method for H_4BPCD (keto form)

reported in (Table S2, supplementary materials). The reactivity order for the nucleophilic case as N(37) > > N(36) > C(35) > S(31). The calculated f_k^- value predicts that the possible sites for electrophilic attack is S(18) > O(19) > N(11) > N(12) site and the radical attack was predicted as S(18) and O(19) site.

While the results for the ligand in Keto form (Table 3S, supplementary materials). predict the highest f_k^+ and f_k^- for S(31) followed by O(30) in case of nucleophilic attack while C(35) in case of electrophilic attack. The radical attack was predicted as C(33) > C(35) > S(18) > C(10). In $[Fe_2(BPCD)Cl_2(H_2O)_4].5H_2O$ complex (Table S4, supplementary materials) Fe(40) has the highest f_k^+ value. The reactivity order for the nucleophilic case is Fe(40) > Cl(41) > O(19) > C(13). The calculated f_k^- value predicts that the possible sites for electrophilic attack is S(31) > O(30) > Cl(42) site and the radical attack was predicted at Cl(42) site.

In $[Mn_2(H_3BPCD)Cl_3(H_2O)_3].3H_2O$ the most favored site (Table S5, supplementary materials). for the nucleophilic, electrophilic and radical attack is C(9), Cl(35) and S(18) respectively. Moreover, the most favored site for the nucleophilic and attack In $[Cr_2(BPCD)Cl_2(H_2O)_4].H_2O$ complex (Table 6S, supplementary materials) is S(31) and for radical attack is O(49). The ability of attack sites in H_4BPCD and its complexes are listed in Table 7.

Mulliken population analysis We use the formalism due to Mulliken in order to perform the population analysis.[81] Mulliken Population Method can be used for explaining and predicting the reactive behavior of a wide set of chemical systems and the nature of the chemical bond.[82,83] Mulliken atomic charges calculated by DFT method is collected and shown by the corresponding Mulliken's plots (Figure 15). It is worthy to mention that C(15), C(13), N(12), N(11), O(19) and S(18) atoms of H_4BPCD (enol form) exhibit positive value, while C(23), C(29), N(34), C(11), O(38), S(31), N(36) and N(37) exhibit negative charge. N(37) of azomethane$_1$ group has a maximum negative charge value. On the other hand, the maximum positive atomic charge is obtained for S(18) of (C=S) group. For the keto form C(21), C(9), O(19), C(10), S(18) and C(33) atoms exhibit positive charge, while C(29), N(11), C(13), C(16), O(30), O(38) and S(31) atoms exhibit negative charges. S(31) of (C=S) group

TABLE 6 Calculated E_{HOMO}, E_{LUMO}, energy band gap ($E_H - E_L$), chemical potential (μ), electronegativity (χ), global hardness (η), global softness (S), global electrophilicity index (ω) and softness (б), ionization potential (I) and electron affinity (A) for H_4BPCD and its metal complexes

Compound	E_{HUMO} (eV)	E_{LUMO} (eV)	ΔE (eV)	χ (eV)	μ (eV)	η (eV)	S (eV^{-1})	ω (eV)	б (eV^{-1})	A (eV)	I (eV)
H_4BPCD (enol form)	−4.897	−4.000	0.897	4.448	−4.448	0.448	1.115	22.064	2.230	4.000	4.897
H_4BPCD (keto form)	−5.136	−3.979	1.157	4.558	−4.558	0.578	0.865	17.960	1.729	3.979	5.136
$[Fe_2(BPCD)Cl_2(H_2O)_4].5H_2O$	−5.662	−4.593	1.070	5.128	−5.128	0.535	0.935	24.579	1.870	4.593	5.662
$[Mn_2(H_3BPCD)Cl_3(H_2O)_3].3H_2O$	−5.562	−4.087	1.475	4.825	−4.825	0.737	0.678	15.783	1.356	4.087	5.562
$[Cr_2(BPCD)Cl_2(H_2O)_4].H_2O$	−5.936	−3.899	2.037	4.917	−4.917	1.018	0.491	11.872	0.982	3.899	5.936

TABLE 7 Ordering the nucleophilic, electrophilic and radical attack sites for H_4BPCD and its metal complexes

Compound	Nucleophilic attack	Electrophilic attack	Radical attack
H_4BPCD_{enol}	N(37) > > N(36) > C(35) > S(31)	S(18) > O(19) > N(11) > N(12)	S(18)> > O(19) > N(11) > N(12)
H_4BPCD_{keto}	S(31) > O(30) > C(13) > O(38)	C(35) > C(10) > C(33) > S(18)	C(33) > C(35) > S(18) > C(10)
$[Fe_2(BPCD)Cl_2(H_2O)_4].5H_2O$	Fe(40) > Cl(41) > O(19) > C(13)	S(31) > O(30) > Cl(42)	Cl(42) > Cl(41) > S(31) > S(18)
$[Mn_2(H_3BPCD)Cl_3(H_2O)_3].3H_2O$	C(9) > C(15) = Mn(47) > C(13)	Cl(51) > S(31) > S(18) > N(34)	S(18) > S(31) > Cl(51) > C(13)
$[Cr_2(BPCD)Cl_2(H_2O)_4].H_2O$	S(31) > Cr(39) > Cl(43) > S(18)	S(31) > S(18) > O(17) > O(44)	O(49) > C(13) > N(36) = N(37)

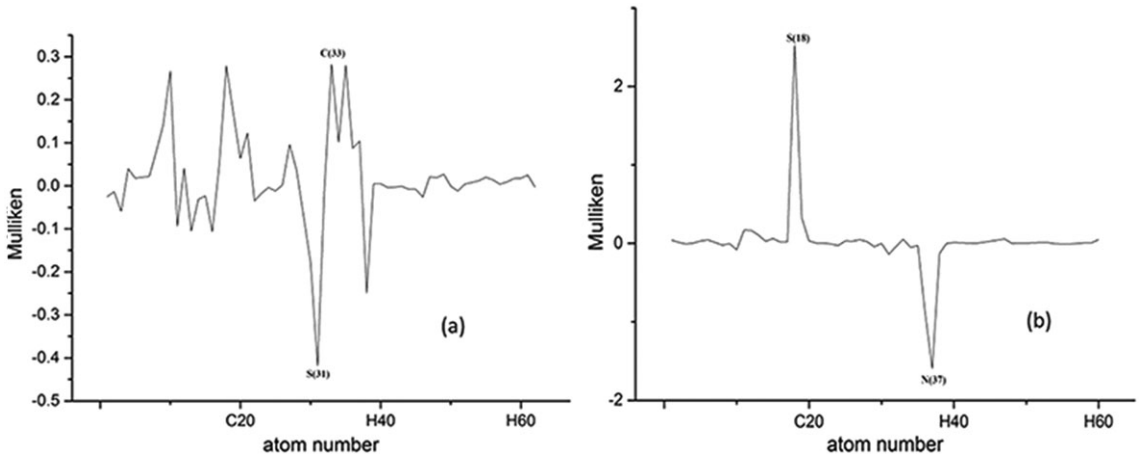

FIGURE 15 The Mulliken diagram distribution of a) H_4BPCD_{keto}, b) H_4BPCD_{enol}

has the greatest values of negative charge, while the highest positive atomic charge is obtained for C(33) of $(C=O)_2$ group.

For the keto form C(21), C(9), O(19), C(10), S(18) and C(33) atoms exhibit positive charge, while C(29), N(11), C(13), C(16), O(30), O(38) and S(31) atoms exhibit negative charges. S(31) of (C=S) group has a maximum negative charge values, while the maximum positive atomic charge is obtained for C(33) of (C=O)2 group.

3.5.4 | Molecular electrostatic potential (MEP)

MEP correlates with electronegativity, partial charges and chemical reactivity of the molecules.[84–87] MEP maps of H_4BPCD in enol and keto form have been observed in two different planes (Figures 16 and 17, respectively) for each molecule. The different values of the electrostatic potential at the surface are represented by different colors: red color symbolize to regions of most negative electrostatic potential which preferred site for electrophilic attack and blue color symbolize to regions of most positive electrostatic potential which preferred site for nucleophilic attack. An increase in potential has the order: red< orange < yellow < green < blue. The color scale of the map ranges from −0.12278 to 0.14147 kcal/mol in enol form, while in keto form −0.0018995 to 0.79213 kcal/mol.

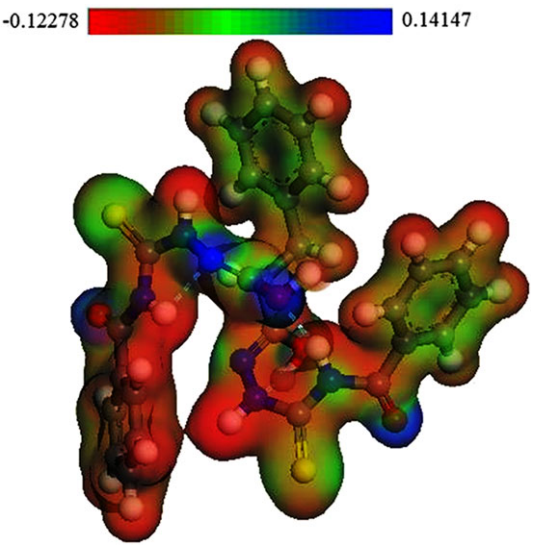

FIGURE 16 Molecular electrostatic potential map for H_4BPCD_{enol}

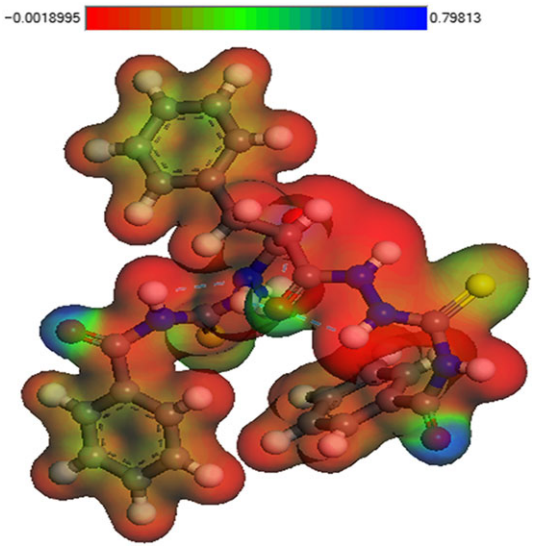

FIGURE 17 Molecular electrostatic potential map for H_4BPCD_{keto}

3.6 | Thermogravimetric studies

All synthesized complexes are subjected to the (TG) and the 1st derivative (DTG) analysis within temperature rang 22–800 °C in nitrogen flow to understanding their thermal stability, hydrated and coordinated water molecules as well as a general pattern for their thermal decomposition steps. Moreover, TGA data provides remarkable information about the water molecules within the complexes complementary to the elemental analyses. Generally, thermal degradation of the complexes takes place in three major steps:

I. Removal of the hydrated water from about 22 to 108 °C, and resumes from about 108 to 244 °C for coordinated water.
II. Depending on the nature of each complex, the degradation process of the ligand part starts mostly from about 243 °C. The weight loss at this step may attribute to the evolution of gases such as CO_2, H_2S, N_2, SO_2, NO_2 or HCl.
III. The last step of decomposition process belongs to the strongly bound fragment of the remaining organic molecule, which includes the removal of the metal sulfide or metal oxide. Finally, the thermogram shows stability until 800 °C (Figures 18–20).

3.7 | Kinetic data

The thermal stability of the chelated have been analyzed in terms of decomposition kinetic parameters derived from Broido (B),[88] the integral method using the Coats-Redfern (CR) equation[89] and the approximation method using the Horowitz- Metzger (HM) equation[90] (Table 8). The 1st decomposition step of Fe (III)-complex which calculated by three methods was graphed in Figure 21 as representative example. The next steps of this complex in addition to the whole decomposition process of other complexes were represented in Figures S8-S16, supplementary materials. Generally, all methods used to measure the change in physical properties of compounds such as weight variation as a function of temperature or time. According to the output data the following observations can be illustrated:

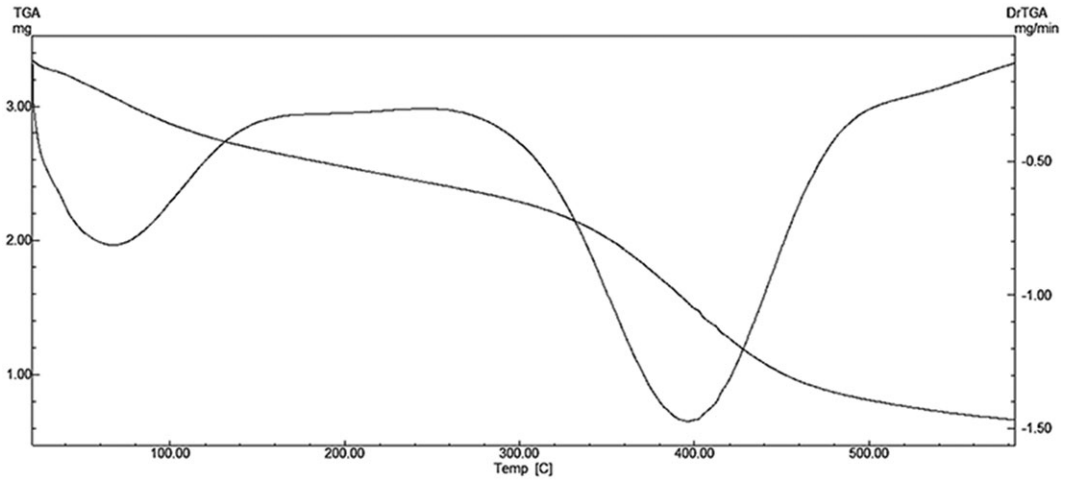

FIGURE 18 Thermal analysis curves of $[Cr_2(BPCD)Cl_2(H_2O)_4].H_2O$ complex

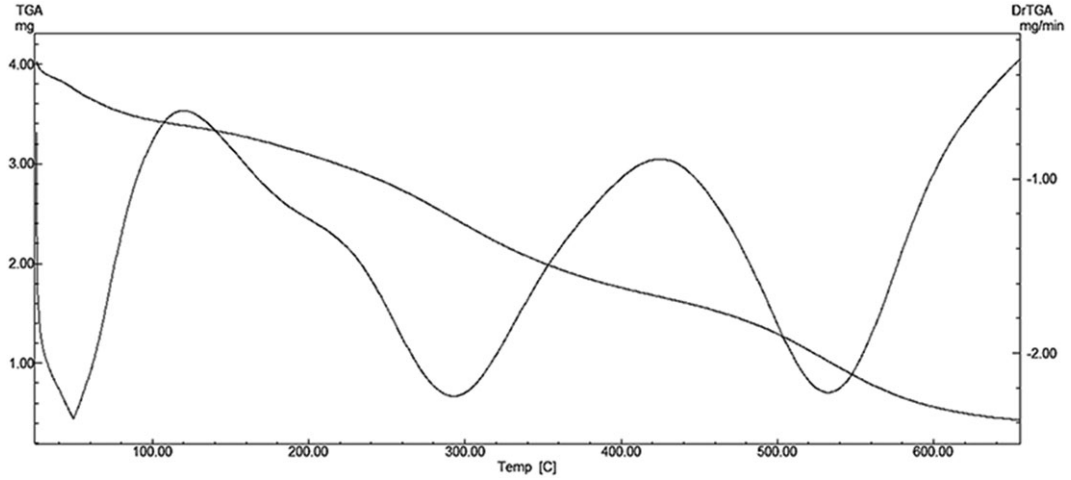

FIGURE 19 Thermal analysis curves of $[Fe_2(BPCD)Cl_2(H_2O)_4].5H_2O$ complex

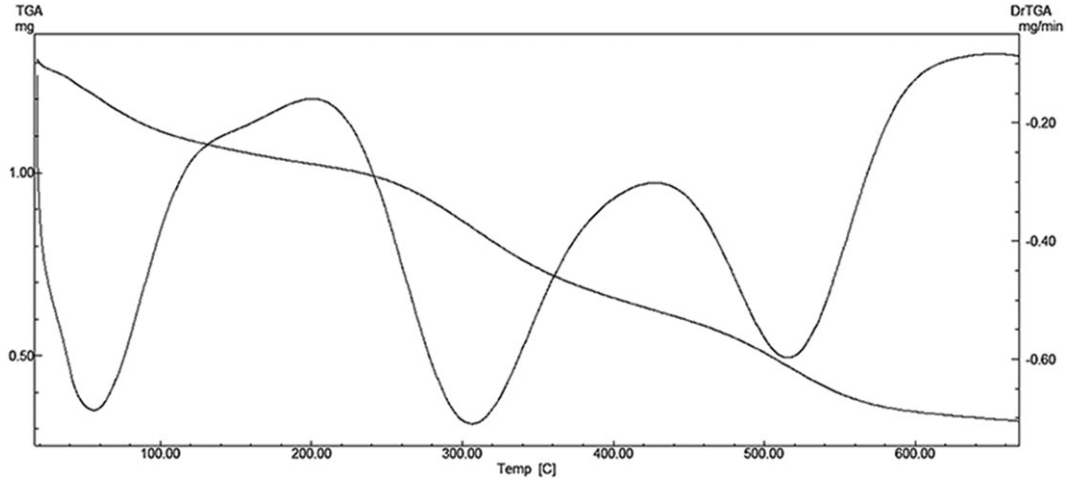

FIGURE 20 Thermal analysis curves of $[Mn_2(H_3BPCD)Cl_3(H_2O)_3].3H_2O$ complex

i. It was inferred that all the thermal decomposition reaction of complexes have the first order, these complexes show similar type of thermal behavior as it shown by E_a and A values of these reactions. The kinetic parameters of different decomposition steps are impacted by type and nature of central metal atoms.
ii. The output E_a values using three variable methods gives different data although difference was found in a narrow range. Over all, the calculation of E_a using Briodo's method gives higher values than the two other methods.[91]
iii. Moreover, the high values of E_a, in complexes, reflects the high stability of the complexes due to their covalent bond character.[92] The E_a values obey the order: Mn (II) > Fe (III) > Cr (III) complex. Consequently, the thermal stability increases in this sequence.
iv. The positive values of ΔG* of the degradation processes indicate their non-spontaneously nature and for the concerning complexes the value increases from one step to another so that the values of TΔS overweight the values of ΔH*.[93–95]

The negative value of ΔS* (entropy of activation) in all complexes due to the lower rate and slow of decomposition reactions than the natural ones. The high degree of ordered is controlled by the polarization of bonds in the activated state which occur by electronic transition and charge migrations.[96] The positive sign in few decomposition steps may attributed to that the reaction produces more gas molecules than it consumes.

v. Comparison of the three sets of kinetic parameters show no significant difference between them.[91]

TABLE 8 Kinetic Parameters evaluated by Horowitz- Metzger, Coats-Redfern and Broido equations for Fe (III), Mn (II) and Cr (III) complexes of H_4BPCD

Compound	step	Mid Temp.(K)	Method	E_a KJ\mol	A (S^{-1})	ΔH* KJ\mol	ΔS* KJ\mol. K	ΔG* KJ\mol
$[Cr_2(BPCD)Cl_2(H_2O)_4].H_2O$	1st	299.66	HM	244.29	2.41×10^{40}	241.79	−0.528	83.54
			CR	247.79	1.00×10^{41}	245.31	−0.539	83.50
			B	258.4	5.8×10^{43}	255.91	−0.593	78.26
	2nd	346.67	HM	59.73	4.81×10^{6}	56.85	−0.118	97.84
			CR	55.25	1.09×10^{6}	52.37	−0.131	97.62
			B	62.41	2.56×10^{6}	59.52	−0.104	95.69
	3rd	660.41	HM	129.77	5.08×10^{7}	124.28	−0.104	192.96
			CR	121.76	1.26×10^{7}	116.27	−0.116	192.59
			B	135.77	3.29×10^{7}	130.28	−0.088	188.70
	4th	774.33	HM	633.21	1.49×10^{41}	626.77	0.535	212.23
			CR	610.78	4.51×10^{39}	604.34	0.506	212.30
			B	637.19	1.87×10^{40}	630.76	0.537	214.74
$[Fe_2(BPCD)Cl_2(H_2O)_4].5H_2O$	1st	316.95	HM	88.52	5.3×10^{12}	85.88	−0.002	86.46
			CR	84.17	1.06×10^{12}	81.53	−0.015	86.34
			B	89.45	9.31×10^{12}	86.82	−0.002	85.91
	2nd	553.62	HM	92.72	1.77×10^{6}	88.12	−0.130	160.33
			CR	88.43	7.66×10^{5}	83.83	−0.137	159.88
			B	97.35	9.50×10^{6}	92.75	−0.116	157.23
	3rd	758.7	HM	315.19	5.66×10^{18}	308.88	0.106	228.21
			CR	330.56	6.53×10^{19}	324.25	0.127	228.15
			B	343.71	5.1×10^{20}	337.40	0.163	213.81
	4th	829.97	HM	450.09	2.59×10^{26}	443.19	−0.252	233.85
			CR	436.49	3.67×10^{25}	429.59	−0.236	233.73
			B	450.28	2.63×10^{26}	443.38	−0.252	233.93
$[Mn_2(H_3BPCD)Cl_3(H_2O)_3].3H_2O$	1st	312.16	HM	67.05	1.24×10^{9}	64.45	−0.071	86.68
			CR	64.51	5.02×10^{8}	61.91	−0.079	86.49
			B	69.78	6.5×10^{9}	67.19	−0.057	85.10
	2nd	348.4	HM	196.27	1.88×10^{27}	193.37	−0.276	97.24
			CR	198.96	4.89×10^{27}	196.06	−0.284	97.16
			B	204.87	1.61×10^{28}	201.97	−0.313	92.94
	3rd	555.35	HM	144.68	9.17×10^{10}	140.07	−0.040	162.39
			CR	147.78	1.91×10^{11}	143.17	−0.034	162.12
			B	157.39	6.14×10^{12}	152.78	−0.005	155.69
	4^{th}	812.8	HM	352.61	6.7×10^{20}	345.85	0.145	227.63
			CR	334.12	4.37×10^{19}	327.37	0.123	227.59
			B	347.52	2.11×10^{20}	340.52	0.136	230.37

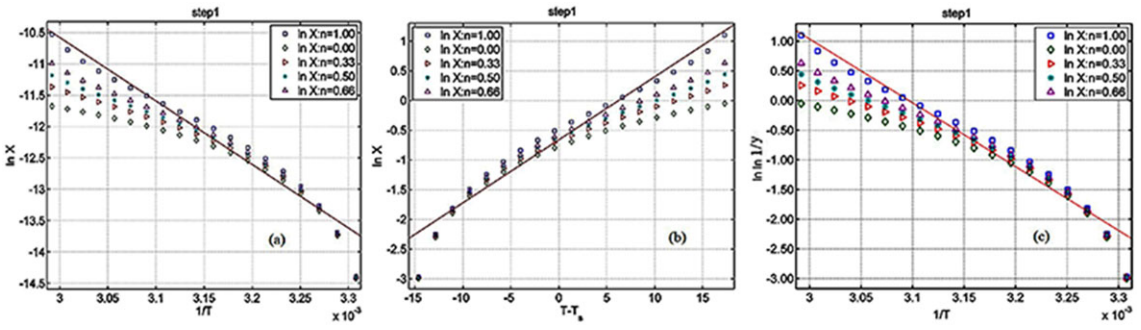

FIGURE 21 1st degradation step for $[Fe_2(BPCD)Cl_2(H_2O)_4].5H_2O$ complex by a) Coats-Redfern method. b) Horowitz-Metzger method. c) Broido method

3.8 | Biological studies and molecular docking

3.8.1 | Determination of minimum inhibitory concentration (MIC)

Importance of MIC arises clearly in symptomatic research centers to confirm resistance of microorganisms to antimicrobial agents, in addition, to control the activity of new antimicrobial agents. The isolated compounds were initially evaluated for *in vitro* antibacterial activity against G + ve and G-ve bacteria and fungal using Broth method.[97] Standard antibiotic namely Ampicillin and standard antifungal drug Clotrimazole were applied as reference drugs. On the basis of the data obtained and listed in Table 9 (Figure 22). A glance of data indicates that:

i. H_4BPCD and $[Fe_2(BPCD)Cl_2(H_2O)_4].5H_2O$ were effective against all organisms, but the parent ligand was the most effective.
ii. $[Cr_2(BPCD)Cl_2(H_2O)_4].H_2O$ exhibited both antibacterial and antifungal activities towards *S. aureus* and *C. Albicans* respectively.
iii. $[Mn_2(H_3BPCD)Cl_3(H_2O)_3].3H_2O$ show moderate activity against *C. Albicans* only.
iv. Finally, the negative results can be explained either to the disability of the compounds to diffuse through the cell wall of the bacterium and/or fungi organisms, and hence couldn't interfere with its biological activity or they can diffuse and inactivated by unknown cellular mechanism.

TABLE 9 Minimal inhibitory concentration (MIC, μg/ml) of the newly synthesized compounds

Compound	*E. coli*	*S. aureus*	*C. Albicans*
Ampicillin	125	93.7	----
Clotrimazole	----	----	5.8
H_4BPCD	187.5	125	23.4
$[Fe_2(BPCD)Cl_2(H_2O)_4].5H_2O$	750	750	750
$[Mn_2(H_3BPCD)Cl_3(H_2O)_3].3H_2O$	NA	NA	750
$[Cr_2(BPCD)Cl_2(H_2O)_4].H_2O$	NA	750	375

NA = no activity

3.8.2 | Antioxidant activity (determination of SOD-like activity)

Within a cell, the superoxide dismutases (SODs) constitute the first line of defense against ROS.[98] Therefore, SOD mimics have these great attention potential pharmaceutical agents for treating such diseases. A significant SOD-like activity was observed for H_4BPCD as represented in Table 10, with inhibition percent 77.3%. Since iron is a most relevant metal for the design of synthetic SOD catalysts,[99] $[Fe_2(BPCD)Cl_2(H_2O)_4].5H_2O$ shows high SOD-like activity as inhibition percent 70.1% followed by $[Cr_2(BPCD)Cl_2(H_2O)_4].H_2O$ with 63.5% percent. $[Mn_2(H_3BPCD)Cl_3(H_2O)_3].3H_2O$ exhibited lowest SOD-like activity (33.1%). Therefore, H_4BPCD and

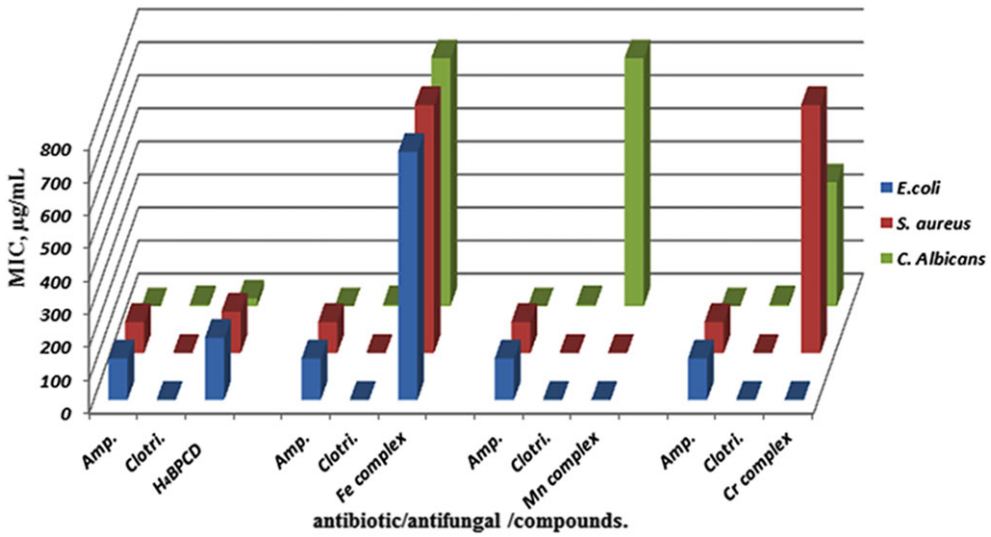

FIGURE 22 Comparison of MIC (mg/ml) of prepared compounds with standard antibiotics and antifungal drug: Amp. (Ampicillin); Clotri. (Clotrimazole)

TABLE 10 Superoxide (SOD)-like activity of the metal complex as antioxidative enzyme

Compound	Δ through 5 min	% inhibition
Control	0.468	0%
L-Ascorbic acid	0.101	78.4%
H_4BPCD	0.106	77.3%
$[Fe_2(BPCD)Cl_2(H_2O)_4].5H_2O$	0.140	70.1%
$[Mn_2(H_3BPCD)Cl_3(H_2O)_3].3H_2O$	0.313	33.1%
$[Cr_2(BPCD)Cl_2(H_2O)_4].H_2O$	0.171	63.5%

% inhibition = (ΔControl- ΔTest/ΔControl) × 100

$[Fe_2(BPCD)Cl_2(H_2O)_4].5H_2O$ complex can be used as antioxidants.

3.8.3 | DNA-binding affinity and docking studies

The displacement was determined by a spectrophotometric assay as a decrease in the absorbance at 630 nm. Mostly all compounds under investigation showed high affinity to DNA which was confirmed by retaining the DNA-compound complex at the origin or by migrating for very short distances. The activity of the compounds follow the order H_4BPCD > $[Fe_2(H_2BPCD)Cl_4(H_2O)_2].5H_2O$ > $[Cr_2(BPCD)Cl_2(H_2O)_4].H_2O$ > $[Mn_2(H_3BPCD)Cl_3(H_2O)_3].3H_2O$. The active compounds were subjected to MG-DNA displacement assay and the results are shown in Table 11. These results are in accordance with the antimicrobial screening data and explain them, suggesting that binding with DNA may contribute to the activity of these compounds against bacterial infections.

The molecular interactions of compounds for inhibition against *E. coli* are represented in Table 12 and Figures 23–26. According to this interaction, H_4BPCD shows interactions with the active site residues and it has the highest glide *E-model* with −186.345 for *E. coli* compared with reference drug, ampicillin (*E-model* = −65,69) (Figures 23 and 24) which similar to experimental DNA-binding affinity. The high affinity

TABLE 11 DNA/methyl green colorimetric assay of the DNA-binding and E-model of ligands (H_4BPCD) and its metal complexes

compound	DNA/methyl green (IC_{50}, μg/ml)	*E-model* (towards E.coli)
H_4BPCD	29.5 ± 1.7	−186.345
$[Cr_2(BPCD)Cl_2(H_2O)_4].H_2O$	65.6 ± 3.5	−47.976
$[Mn_2(H_3BPCD)Cl_3(H_2O)_3].3H_2O$	70.5 ± 3.7	−44.994
$[Fe_2(H_2BPCD)Cl_4(H_2O)_2].5H_2O$	40.2 ± 2.5	--

IC_{50} values represent the concentration (mean ± SD, n = 3–5 separate determinations) required for a 50% decrease in the initial absorbance of the DNA/methyl green solution.

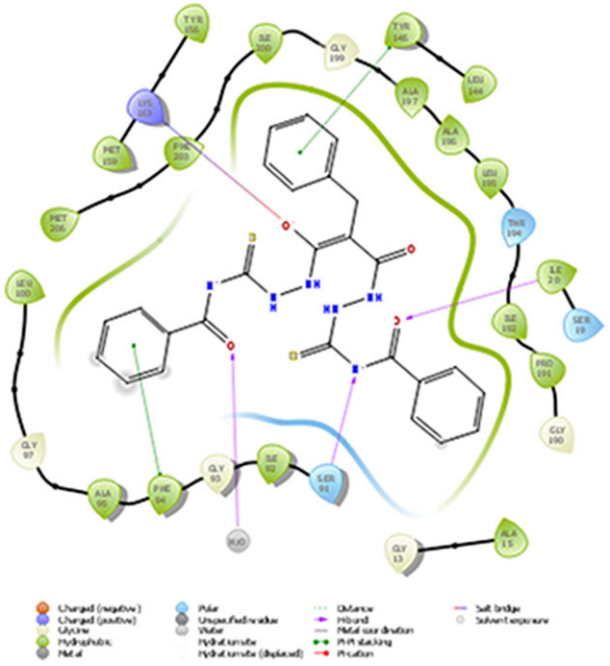

FIGURE 23 2D molecular interaction of H_4BPCD for inhibitor to E. Coli

TABLE 12 Molecular interactions predicted for inhibitor binding to *E.Coli*

Compound	Hydrogen bonds			
	Donor Acceptor	Salt bridge	π-cation	π- π Stacking edge to face
H_4BPCD	ILE20 ➔ (C=O) SER91 ➔ (N^-) H_2O ➔ (C=O)	LYS163--(C-O^-)	----	TYR146 PHE94
$[Cr_2(BPCD)Cl_2(H_2O)_4].H_2O$	H_2O ➔ (C=O)	LYS43---(C-O^-)	LYS43-(Ar ring)	PHE94
$[Mn_2(H_3BPCD)Cl_3(H_2O)_3].3H_2O$	(NH) ➔ SER198	----	----	----

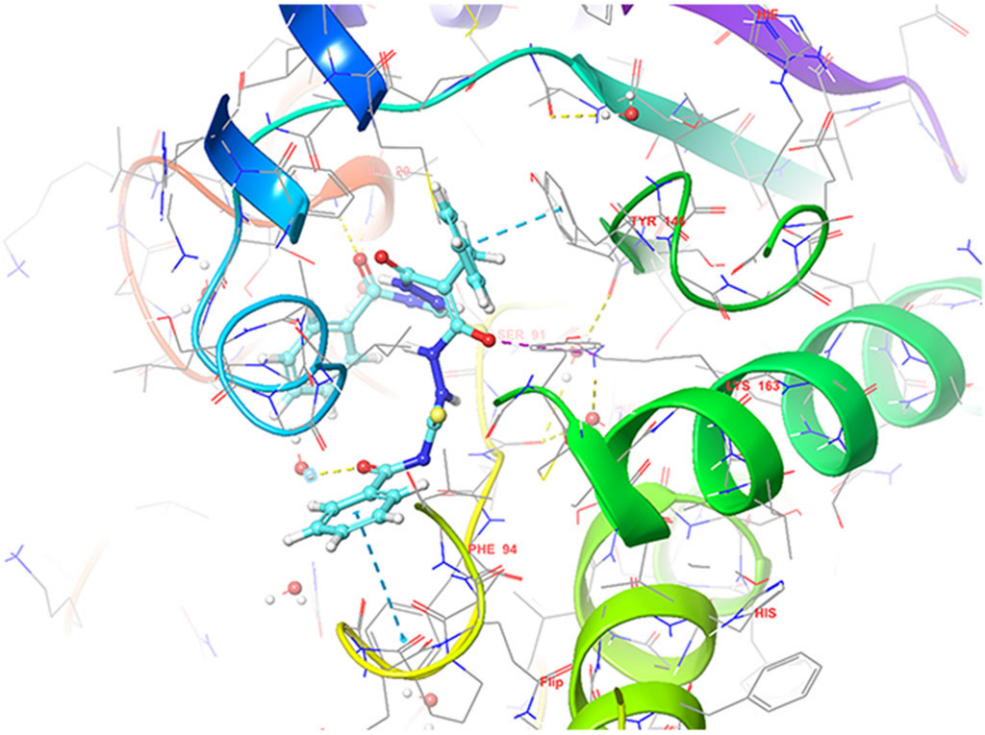

FIGURE 24 3D molecular interaction of H_4BPCD for inhibitor to E. Coli

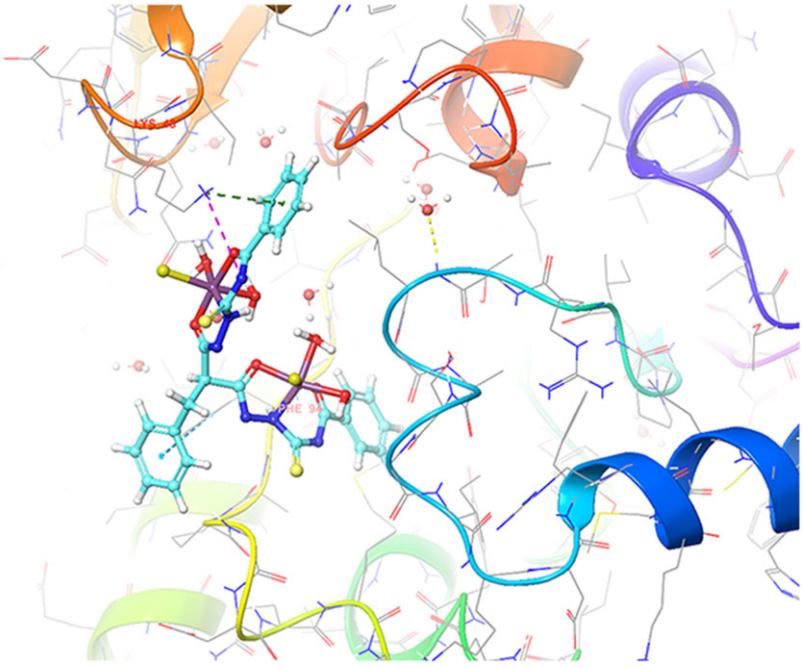

FIGURE 25 3D molecular interaction of $[Cr_2(BPCD)Cl_2(H_2O)_4].H_2O$ for inhibitor to E. Coli

of H_4BPCD against *E.coli* is resulting from interaction via hydrogen bonds [ILE20 ➔ (C=O), SER91 ➔ negative (N^-) and H_2O ➔ (C=O)], Salt bridge between LYS163 and negative oxygen of ($C\text{-}O^-$) as well as π- π stacking edge to face of aromatic rings with TYR146 and PHE94. While, the interaction of $[Cr_2(BPCD)Cl_2(H_2O)_4].H_2O$ (glide *E-model* = −47.98) with *E. coli* (Figure 25) through hydrogen bonds H_2O ➔ (C=O), Salt bridge between LYS43 and negative oxygen of ($C\text{-}O^-$), π-cation between LYS43-(aromatic ring) and π- π stacking edge to face of aromatic ring with PHE94. Furthermore, $[Mn_2(H_3BPCD)Cl_3(H_2O)_3].3H_2O$ shows glide *E-model* = −44.99 with interaction only through hydrogen bond donor (NH) ➔ SER198 (Figure 26).[43] While,

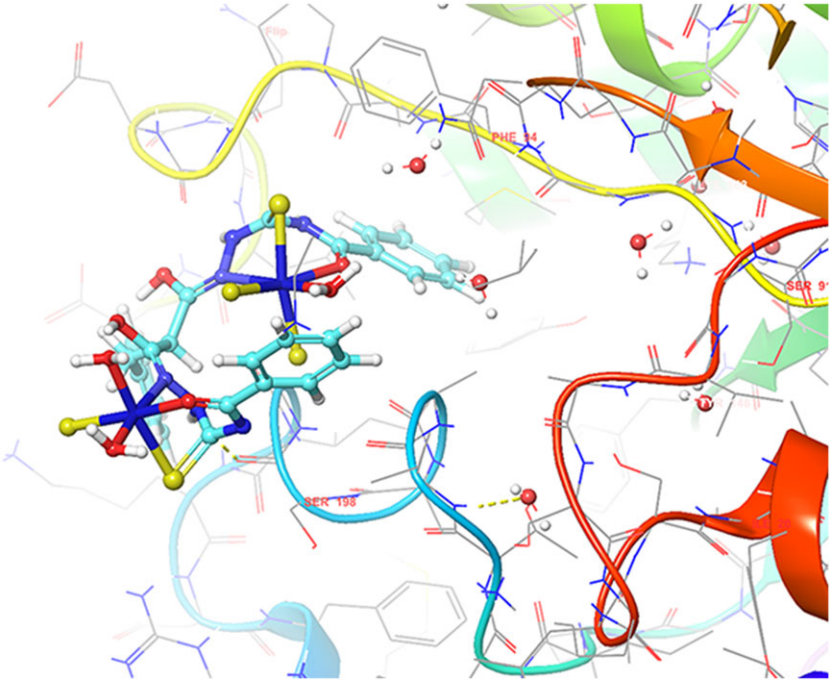

FIGURE 26 3D molecular interaction of $[Mn_2(H_3BPCD)Cl_3(H2O)_3].3H_2O$ for inhibitor to E. Coli

while $[Fe_2(H_2BPCD)Cl_4(H_2O)_2].5H_2O$ hasn't any interaction with *E.coli*.

3.8.4 | Structure activity relationships (SAR's)

From the results of antimicrobial activity of the newly investigated compounds and on correlating by their structures it has been observed that:

I. In general, compounds were active against G + ve more than G-ve bacteria. The higher resistance can be attributed to the different composition of cell-wall membrane.[100]
II. It was observed that Fe (III) complex exhibited moderate activity against tested organisms, followed by Cr (III) complex. This activity might be due to the presence of free C=N groups which is electron donating group. Antimicrobial activity was considerably enhanced by presence of electron donating groups.[101]

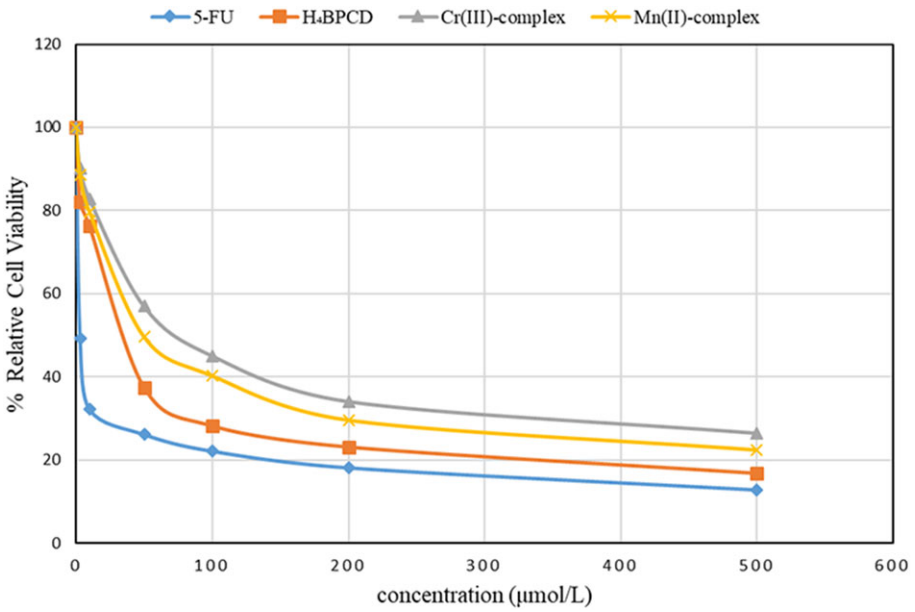

FIGURE 27 MTT-cytotoxicity assay of H_4BPCD and its Cr (III) and Mn (II) complexes

III. The presence of free OH groups in most of the prepared compounds may confer the turbulence of membranous permeability of the bacterial cell-wall through their lateral interactions mediated by H-bonds with it.[102] So it could be an important factor to inhibit the bacterial growth. This may explain why Mn (II) complex have no activity against tested bacteria cause there in no free OH groups in it.

3.8.5 | MTT-cytotoxicity assay

In our experiments, IC_{50} values (compound concentration that produces 50% of cell death) in micro molar units were calculated. For comparison purposes, the cytotoxicity of Fluorouracil (5-FU) and the free ligand as well as its complexes has been evaluated under the same experimental conditions (Figure 27). It is clearly observed that chelation with metal has no synergistic effect on the cytotoxicity. Importantly, it should be emphasized that the ligand shows good activity with IC_{50} = 37.01 μmol/l relative to that of Fluorouracil (2.95 μmol/l) for HePG2. These gratifying results are encouraging its further screening in vitro. Later on, upon further analysis, the ligand also exhibits considerable cell growth inhibition activity against human liver hepatocellular carcinoma HePG-2 cells. Therefore, its further biological evaluation in vivo as well as studies of mechanism of action is necessary. But the two complexes of Cr (III) and Mn (II) show results of IC_{50} (μmol/l) = 79.12 and 49.46 against (HePG-2), respectively.

4 | CONCLUSION

In this study the vibrational analysis, ^{1}H NMR and ^{13}C NMR spectra of a newly synthesized *N,N′*-(2,2′-(2-benzylmalonyl)bis (hydrazine-1-carbonothioyl)) dibenzamide (H_4BPCD) compound and its binuclear Cr (III), Mn (II) and Fe (III) complexes have been studied. The spectral analysis confirmed the presence of both forms (keto and enol) of H_4BPCD and an octahedral geometry was proposed for all complexes. The optimized geometric parameters and Mulliken population analysis have been calculated by using DFT/DMol^3 method with DNP basis set. A good agreement between the theoretical and experimental vibrations upon the comparison between them. All compounds were screened for DNA binding and the calculated energy band gap showed strong relationship between the value of energy gap and the biological activity. Fe (III) complex exhibited higher antimicrobial activity when compared with other compounds due to an electron donating behavior. The ligand H_4BPCD show greater response than Cr (III) and Mn (II) complexes with human tumor cells of hepatocellular carcinoma (HePG-2). Since of the compounds are good candidate for future pharmacological studies the obtained results will be useful in their use in these areas.

ORCID

Mohammed M. El-Gamil https://orcid.org/0000-0001-5605-2844
Gaber M. Abu El-Reash https://orcid.org/0000-0002-0456-7325

REFERENCES

[1] U. R. Bhagavatula, S. Pulipaka, S. Atreyapurapu, *Int. Res. J. Pure. Appl. Chem.* **2016**, *11*, 1.

[2] A. Satyanarayana, D. N. Kenie, P. Shyamala, *Acta Chim. Slov.* **2014**, *60*, 807.

[3] L. Tsitsishvili, T. Tsutsunava, K. Y. Ya, *Koord. Khim.* **1982**, *8*, 674.

[4] T. A. Kaden, *Coord. Chem. Rev.* **1999**, *190*, 371.

[5] A. F. Shoair, A. A. El-Bindary, N. A. El-Ghamaz, G. N. Rezk, *J. Mol. Liq.* **2018**, *269*, 619.

[6] H. Steinhagen, G. Helmchen, *Angew. Chem. Int. Ed.* **1996**, *35*, 2339.

[7] E. K. van den Beuken, B. L. Feringa, *Tetrahedron* **1998**, *54*, 12985.

[8] E. Authority, *EFSA J.* **2015**, *13*, 3991.

[9] M. V. Angelusiu, S. -F. Barbuceanu, C. Draghici, G. L. Almajan, *Eur. J. Med. Chem.* **2010**, *45*, 2055.

[10] H. G. Aslan, S. Özcan, N. Karacan, *Inorg. Chem. Commun.* **2011**, *14*, 1550.

[11] Z. -h. Xu, X. -w. Zhang, W. -q. Zhang, Y. -h. Gao, Z. -z. Zeng, *Inorg. Chem. Commun.* **2011**, *14*, 1569.

[12] H. A. Sahyon, A. A. El-Bindary, A. F. Shoair, A. A. Abdellatif, *J. Mol. Liq.* **2018**, *255*, 122.

[13] M. Khalifa, *Analysis* **1995**, *23*, 453.

[14] O. A. El-Gammal, F. E. El-Morsy, B. Jeragh, A. A. El-Asmy, *Can. Chem.Transac.* **2013**, *1*, 277.

[15] M. A. Kabil, M. A. Akl, M. E. Khalifa, *Anal. Sci.* **1999**, *15*, 433.

[16] M. Katyal, Y. Dutt, *Talanta* **1975**, *22*, 151.

[17] A. Cameron, N. Gibson, R. Roper, *Anal. Chim. Acta* **1963**, *29*, 73.

[18] C. Bell, D. Rose, *Talanta* **1965**, *12*, 696.

[19] J. Sears, J. Darby, Mechanism of plasticizer action, in *The Technology of Plasticizers*, (Ed: N. Platzer), Wiley-Interscience, New York **1982** 35.

[20] E. Massarani, D. Nardi, A. Tajana, L. Degen, *J. Med. Chem.* **1971**, *14*, 633.

[21] L. Troian-Gautier, C. Moucheron, *Molecules* **2014**, *19*, 5028.

[22] G. R. Reddy, S. Balasubramanian, *RSC Adv.* **2015**, *5*, 53979.

[23] D. Ayodhya, M. Venkatesham, A. S. Kumari, G. B. Reddy, D. Ramakrishna, G. Veerabhadram, *J. Fluorescence* **2015**, *25*, 1481.

[24] A. Guha, J. Adhikary, T. K. Mondal, D. Das, **2011**.

[25] A. A. Adeniyi, K. S. Patel, *Synth. React. Inorg. Met. Org. Chem.* **1993**, *23*, 199.

[26] *Modeling and Simulation Solutions for Chemicals and Materials Research*, BIOVIA Materials Studio, Accelrys software Inc., San Diego, USA **2017**.

[27] S. M. Bridges, M. L. Salin, *Plant Physiol.* **1981**, *68*, 275.

[28] Z. A. Siddiqi, M. Shahid, M. Khalid, S. Kumar, *Eur. J. Med. Chem.* **2009**, *44*, 2517.

[29] A. I. Vogel, *Vogel's Textbook of Quantitative Chemical Analysis*, 5th ed., John Wiley & Sons, New York **1991**.

[30] X. Wu, A. K. Ray, *Phys. Rev. B* **2002**, *65*, 085403.

[31] B. Delley, D. Ellis, A. Freeman, E. Baerends, D. Post, *Phys. Rev. B* **1983**, *27*, 2132.

[32] B. Hammer, L. B. Hansen, J. K. Nørskov, *Phys. Rev. B* **1999**, *59*, 7413.

[33] A. Matveev, M. Staufer, M. Mayer, N. Rösch, *Int. J. Quantum Chem.* **1999**, *75*, 863.

[34] R. Taylor, N. Manandhar, G. Towers, *J. Ethnopharmacol.* **1995**, *46*, 153.

[35] A. K. Sadana, Y. Mirza, K. R. Aneja, O. Prakash, *Eur. J. Med. Chem.* **2003**, *38*, 533.

[36] N. S. Burres, A. Frigo, R. R. Rasmussen, J. B. McAlpine, *J. Nat. Prod.* **1992**, *55*, 1582.

[37] M. C. Alley, D. A. Scudiero, A. Monks, M. L. Hursey, M. J. Czerwinski, D. L. Fine, B. J. Abbott, J. G. Mayo, R. H. Shoemaker, M. R. Boyd, *Cancer Res.* **1988**, *48*, 589.

[38] D. A. Scudiero, R. H. Shoemaker, K. D. Paull, A. Monks, S. Tierney, T. H. Nofziger, M. J. Currens, D. Seniff, M. R. Boyd, *Cancer Res.* **1988**, *48*, 4827.

[39] X. Qiu, S. S. Abdel-Meguid, C. A. Janson, R. I. Court, M. G. Smyth, D. J. Payne, *Protein Sci.* **1999**, *8*, 2529.

[40] Schrödinger Suite 2017–1: Schrödinger Suite 2017-1, Protein Preparation Wizard; Epik, Schrödinger, LLC, New York, NY, **2017**; Impact, Schrödinger, LLC, New York, NY, **2017**; Prime, Schrödinger, LLC, New York, NY, **2017**.

[41] Schrödinger Suite 2017–1: LigPrep, Schrödinger, LLC, New York, NY, **2017**.

[42] Schrödinger Suite 2017–1: Glide, Schrödinger, LLC, New York, NY, **2017**.

[43] G. Jagadeesan, V. Vijayakuma, M. Palayam, G. Suresh, G. Krishnaswamy, S. Aravindhan, G. H. Peters, *J Proteomics Bioinformatics* **2015**, *8*, 142.

[44] T. A. Yousef, G. M. Abu El-Reash, R. M. El Morshedy, *Polyhedron* **2012**, *45*, 71.

[45] T. A. Yousef, G. M. Abu El-Reash, R. M. El Morshedy, *J. Mol. Struct.* **2013**, *1045*, 145.

[46] J. R. Ferraro, *Low-frequency vibrations of inorganic and coordination compounds*, Plenym Press, New York **1971**.

[47] W. Hui, L. Zcnglu, Z. Yulan, W. Shaozu, *Synth. React. Inorg. Met.-Org. Chem.* **1995**, *25*, 1143.

[48] A. A. R. Despaigne, J. G. Da Silva, A. C. M. Do Carmo, O. E. Piro, E. E. Castellano, H. Beraldo, *J. Mol. Struct.* **2009**, *920*, 97.

[49] O. El-Gammal, G. A. El-Reash, M. El-Gamil, *Spectrochim. Acta A* **2012**, *96*, 444.

[50] T. S. Lobana, P. Kumari, G. Hundal, R. J. Butcher, A. Castineiras, T. Akitsu, *Inorg. Chim. Acta* **2013**, *394*, 605.

[51] T. S. Lobana, A. Sánchez, J. S. Casas, A. Castiñeiras, J. Sordo, M. S. García-Tasende, E. M. Vázquez-López, *J. Chem. Soc., Dalton Trans.* **1997**, 4289.

[52] D. H. Williams, I. Fleming, *Spectroscopic Methods in Organic Chemistry*, fourth ed., McGraw-Hill, London **1989**.

[53] R. M. Silverstein, G. C. Bassler, T. C. Morrill, *Spectrometric identification of organic compounds*, third ed., John Wiley & Sons, New York **1974**.

[54] T. Yousef, G. M. Abu El-Reash, T. Rakha, U. El-Ayaan, *Spectrochim. Acta A* **2011**, *83*, 271.

[55] F. A. Cotton, G. Wilkinson, C. A. Murillo, M. Bochmann, R. Grimes, *Advanced inorganic chemistry*, Wiley Interscience, New York **1988**.

[56] M. Omar, G. G. Mohamed, A. A. Ibrahim, *Spectrochim. Acta A* **2009**, *73*, 358.

[57] P. G. Centre, T. G. Narenda, B. N. Murthy, *Indian J. Chem., Sect A* **1989**, *28*, 689.

[58] M. M. Mostafa, M. A. Khattab, K. M. Ibrahim, *Polyhedron* **1983**, *2*, 583.

[59] O. A. El-Gammal, G. M. Abu El-Reash, S. E. Ghazy, A. H. Radwan, *J. Mol. Struct.* **2012**, *1020*, 6.

[60] D. X. West, J. K. Swearingen, J. Valdés-Martínez, S. Hernández-Ortega, A. K. El-Sawaf, F. van Meurs, A. Castiñeiras, I. Garcia, E. Bermejo, *Polyhedron* **1999**, *18*, 2919.

[61] I. Fleming, *Frontier Orbitals and Organic Chemical Reactions*, Wiley, New York **1976**.

[62] E. Kavitha, N. Sundaraganesan, S. Sebastian, *Indian J. Pure Appl. Phys.* **2010**, *48*, 20.

[63] A. Jayaprakash, V. Arjunan, S. Mohan, *Spectrochim. Acta A* **2011**, *81*, 620.

[64] M. Mohan, M. Kumar, *Transition Met. Chem.* **1985**, *10*, 255.

[65] A. Singh, P. Singh, *Indian J. Chem., Sect. A: Inorg., Bio-Inorg., Phys., Theor. Anal. Chem.* **2000**, *39*, 874.

[66] A. M. Asiri, M. Karabacak, M. Kurt, K. A. Alamry, *Spectrochim. Acta A* **2011**, *82*, 444.

[67] B. Kosar, C. Albayrak, *Spectrochim. Acta A* **2011**, *78*, 160.

[68] K. Chaitanya, *Spectrochim. Acta A* **2012**, *86*, 159.

[69] R. G. Pearson, *J. Org. Chem.* **1989**, *54*, 1423.

[70] J. Padmanabhan, R. Parthasarathi, V. Subramanian, P. Chattaraj, *J. Phys. Chem. A* **2007**, *111*, 1358.

[71] J. C. Rienstra-Kiracofe, G. S. Tschumper, H. F. Schaefer, S. Nandi, G. B. Ellison, *Chem. Rev.* **2002**, *102*, 231.

[72] R. Parthasarathi, V. Subramanian, D. Roy, P. Chattaraj, *Biorg. Med. Chem.* **2004**, *12*, 5533.

[73] S. Sagdinc, B. Koksoy, K. F, S. H. Bayari, *J. Mol. Struct.* **2009**, *917*, 63.

[74] R. G. Pearson, *Proc. Natl. Acad. Sci. U.S.A.* **1986**, *83*, 8440.

[75] T. A. Yousef, O. K. Alduaij, G. M. Abu El-Reash, R. M. El Morshedy, *J. Mol. Liq.* **2016**, *222*, 762.

[76] M. S. Masoud, A. E. Ali, M. A. Shaker, G. S. Elasala, *Spectrochim. Acta Part A* **2012**, *90*, 93.

[77] R. G. Parr, L. V. Szentpaly, S. Liu, *J. Am. Chem. Soc.* **1999**, *121*, 1922.

[78] R. G. Parr, W. Yang, *J. Am. Chem. Soc.* **1984**, *106*, 4049.

[79] W. Yang, R. G. Parr, R. Pucci, *J. Chem. Phys.* **1984**, *81*, 2862.

[80] P. W. Ayers, M. Levy, *Theor. Chem. Acc.* **2000**, *103*, 353.

[81] R. Mulliken, *J. Chem. Phys.* **1955**, *23*, 1841.

[82] M. Segall, R. Shah, C. Pickard, M. Payne, *Phys. Rev. B* **1996**, *54*, 16317.

[83] T. H. Rakha, O. A. El-Gammal, H. M. Metwally, G. M. Abu El-Reash, *J. Mol. Struct.* **2014**, *1062*, 96.

[84] E. Scrocco, J. Tomasi, Electronic Molecular Structure, Reactivity and Intermolecular Forces: An Euristic Interpretation by Means of Electrostatic Molecular Potentials, in *Advances in Quantum Chemistry*, (Ed: L. Per-Olov), Academic Press, New York **1978**, pp. 115.

[85] F. J. Luque, J. M. López, M. Orozco, *Theor. Chem. Acc.* **2000**, *103*, 343.

[86] N. Okulik, A. H. Jubert, *Internet Electron. J. Mol. Des* **2005**, *4*, 17.

[87] S. Chidangil, P. C. Mishra, *J. Mol. Model.* **1997**, *3*, 172.

[88] A. Broido, *J. Polym. Sci. Part A: Polym. Chem.* **1969**, *7*, 1761.

[89] A. W. Coats, J. Redfern, *Nature* **1964**, *201*, 68.

[90] H. H. Horowitz, G. Metzger, *Anal. Chem.* **1963**, *35*, 1464.

[91] K. S. Muralidhara, S. Sreenivasan, *World Appl. Sci. J.* **2010**, *11*, 184.

[92] T. Hatakeyama, F. Quinn. *Thermal Analysis: Fundamentals and Applications to Polymer Science*. John Wiley & Sons, Chichester, England **1999**.

[93] P. Maravalli, T. Goudar, *Thermochim. Acta* **1999**, *325*, 35.

[94] S. S. Kandil, G. B. El-Hefnawy, E. A. Baker, *Thermochim. Acta* **2004**, *414*, 105.

[95] K. K. M. Yusuff, R. Sreekala, *Thermochim. Acta* **1990**, *159*, 357.

[96] J. W. Moore, R. G. Pearson, *Kinetics and mechanism*, third ed., John Wiley & Sons, New York **1961**.

[97] C. M. Atta-ur-Rahman, W. J. Thomsen, *Bioassay techniques for drug development*, Harwood Academic Publishers, The Netherlands **2001**.

[98] D. P. Riley, *Chem. Rev.* **1999**, *99*, 2573.

[99] A. E. Martell, R. J. Motekaitis, *The Determination and Use of Stability Constants*, VCH Publishers, New York **1988**.

[100] M. Salton, *Biochim. Biophys. Acta* **1953**, *10*, 512.

[101] J. Fu, K. Cheng, Z.-m. Zhang, R.-q. Fang, H.-l. Zhu, *Eur. J. Med. Chem.* **2010**, *45*, 2638.

[102] H. Nikaido, *Microbiol. Mol. Biol. Rev.* **2003**, *67*, 593.

SUPPORTING INFORMATION

Additional supporting information may be found online in the Supporting Information section at the end of the article.

How to cite this article: El-Morshedy RM, El-Gamil MM, Abou-Elzahab MM, Abu El-Reash GM. Spectroscopic investigation, DFT, fluorescence, molecular docking and biological studies of divalent and trivalent binuclear complexes prepared from benzoyl thiosemicarbazide derivative of 2-benzylmalonohydrazide. *Appl Organometal Chem*. 2019;e4871. https://doi.org/10.1002/aoc.4871